

Cascaded Optomechanical Sensing for Small Signals

Marta Maria Marchese,¹ Daniel Braun,² Stefan Nimmrichter,^{3,*} and Dennis Rätzel^{4,5,*}

¹*Institute of Science and Technology Austria (ISTA), 3400 Klosterneuburg, Austria*

²*Institute for Theoretical Physics, Eberhard Karls Universität Tübingen,*

Auf der Morgenstelle 14, 72076 Tübingen, Germany

³*Naturwissenschaftlich-Technische Fakultät, Universität Siegen, Walter-Flex-Straße 3, 57068 Siegen, Germany*

⁴*Department of Physics and Astronomy, University College London,*

Gower Street, WC1E 6BT London, United Kingdom

⁵*ZARM, University of Bremen, Am Fallturm 2, 28359 Bremen, Germany*

We propose a sensing scheme for detecting weak forces that achieves Heisenberg-limited sensitivity without relying on entanglement or other non-classical resources. Our scheme utilizes coherent averaging across a chain of N optomechanical cavities, unidirectionally coupled via a laser beam. As the beam passes through the cavities, it accumulates phase shifts induced by a common external force acting on the mechanical elements. Remarkably, this fully classical approach achieves the sensitivity scaling typically associated with quantum-enhanced protocols, providing a robust and experimentally feasible route to precision sensing. Potential applications range from high-sensitivity gravitational field measurements at the Large Hadron Collider to probing dark matter interactions and detecting gravitational waves. This work opens a new pathway for leveraging coherent light-matter interactions for force sensing.

I. INTRODUCTION

Detecting extremely weak forces with high sensitivity remains a central challenge in modern physics, with broad relevance to both fundamental research and technological development. In fundamental studies, enhanced sensitivity enables the exploration of new physical regimes, including the investigation of gravity at the quantum scale, the search for dark matter candidates, and the examination of the principles underlying quantum mechanics. From a technological perspective, advances in ultra-sensitive force detection underpin the development of precision measurement techniques and sensor technologies with wide-ranging applications.

Optomechanical systems [1] have long been used to tackle diverse questions in quantum mechanics, from the exploration of fundamental physics [2–4] to sensing applications [5–7]. The ground state cooling of the mechanical element and the radiation-pressure interaction with a light field allow to enter a quantum regime where the mechanical motion becomes highly sensitive to small disturbances [8–10]. In this context, optomechanical systems represent ideal platforms to test weak forces as they offer high force sensitivity with many recent advances [11–13]. This opens new paths to unveil and test physical effects, ranging from quantum-gravity signatures [14–18], to dark matter detection [19–21], or measurements

of high-frequency gravitational waves from continuous sources [22].

Improving a detector's sensitivity means making the signal stand out more clearly from background noise. A common method, used even in classical physics, is to average the results over N measurements, either by repeating the same experiment or by collecting data from multiple independent probes. This approach leads to a Signal-to-Noise Ratio (SNR) enhanced by a factor proportional to \sqrt{N} , known as the Standard Quantum Limit (SQL). Quantum correlations between probes can push this improvement even further, reaching what is known as the Heisenberg limit (HL), where the SNR scales linearly with N , the number of probes [23]. Although entanglement and squeezing have demonstrated such gains, their practical use is limited by the fragility of quantum resources under the effects of decoherence, which significantly restrict the number of usable probes in an experiment [24, 25].

The basic idea of coherent averaging [26–28] is to employ a coherent procedure to replace the classical averaging: instead of measuring N probes individually, one lets them interact simultaneously with a common quantum system (“bus”) and eventually reads out the latter. The phase information from the N probes accumulates in the quantum bus, leading to an improvement of the SNR. The first key advantage is that this scheme requires no entanglement or quantum resources to surpass the SQL; even simple product states of the probes are sufficient, and in certain regimes they can achieve full HL scaling. The second advantage is that, precisely because it avoids fragile entangled states, the scheme can be more robust to decoherence, making it significantly more practical in realistic, noisy experimental settings. Among the several other ways that have been found to bypass the entanglement requirement to reach HL sensitivity, we just men-

* These authors share last authorship
 marta.marchese@ist.ac.at
 daniel.braun@uni-tuebingen.de
 dennis.ratzel@ucl.ac.uk
 stefan.nimmrichter@uni-siegen.de

tion non-linear schemes [29, 30], multi-pass schemes [31], or non-unitary encoding of the parameter [32]. In fact, coherent averaging can be seen as an interference phenomenon that also works in the classical wave regime, where it is used for SNR enhancement in multipass microscopy of sensitive samples [33, 34]. In [28] it was suggested for enhancing the sensitivity of measurements of Newton's constant G using a set of classical harmonic oscillators all coupled to a central one.

Here, we propose a sensing scheme that exploits coherent averaging for cascaded optomechanical systems. The systems are connected through a unidirectional optical field that acts as the bus and accumulates all the phase signals before being measured, which achieves Heisenberg-like scaling in the ideal case without photon losses. We show that in presence of losses, even though the N^2 -scaling is lost, there is an enhancement up to an optimal number of systems N_{opt} in comparison to the standard quantum limit. To show the utility of the scheme, we discuss three example applications: (1) detection of gravitational field at LHC, (2) dark matter detection, (3) gravitational waves detection.

The proposed configuration is conceptually analogous to sequential multi-pass schemes, in which precision improves by repeatedly sending light through the same cavity. However, the cascaded system offers a complementary approach in which multiple sensors independently receive the same signal. This may be advantageous in scenarios where a single system cannot be reused, such as when a high-intensity laser pulse induces incoherent absorption, loss, or damage.

We note that the cascaded setup inherently introduces a time delay between consecutive cavities due to light propagation. In other words, the bus receives each probe signal sequentially, seemingly at odds with the assumption of simultaneous probe–bus couplings for coherent averaging. This however depends on the timing of the probe signals. For example, the signal may be imprinted on consecutive mechanical elements with a time delay and the light propagation may be adjusted to exactly match this delay. This can be the case in one of our example applications, the detection of the gravitational field at the LHC. Furthermore, if decoherence of the mechanical elements is happening on a much longer time scale than their oscillation period, simultaneity can effectively be achieved by setting the time delay between two oscillators to match an integer multiple of the mechanical period. On the other hand, should the total delay across the chain remain negligible compared to the mechanical period, the interactions are rendered effectively simultaneous.

In Sec. II we describe the cascaded optomechanical setup and how the signal is imprinted on the motion of the mechanical element in each cavity; by deriving and iterating the input-output relations, we obtain a general recursive formula for the output field amplitude. The solution to this recursive relation is given explicitly in the

following three subsections: in II A for the stroboscopic regime, where the duration of the pulse is short compared to the timescale of the mechanical motion; in II B for the continuous-wave regime, with a long pulse compared to the timescales of both mechanical motion and cavity and also compared to the duration of the mechanical signal; in II C for the continuous-wave regime with a continuous signal, where in contrast to the previous case the duration of the pulse is now shorter than the timescale of the mechanical signal. In Sec. III we introduce the metrological bounds to the signal-to-noise ratio (SNR) for Gaussian states in the weak coupling regime. The results for the three limiting cases are presented in Sec. III A, and the upper bound case obtained when all the cavities are identical in Sec. III B. In Sec. IV we discuss three potential applications of the cascaded sensing scheme: IV A Dark Matter searches, IV B Gravitational waves, and IV C Gravitational field of ultra-relativistic matter. In Sec. V we draw our conclusions and outline possible directions for future work.

II. CASCADED OPTOMECHANICS

We implement a coherent-averaging scheme to detect weak signals encoded as phase shifts in mechanical resonators. The system, shown in Fig. 1, consists of N optomechanical cavities, acting as parameter-dependent probes. They are uni-directionally coupled through laser light that serves as a common “quantum bus”. By fixing the initial polarization and inserting polarizing beam splitter (PBS) and quarter wave plates (QWP) (or alternatively Faraday rotators) along the path, it is possible to drive the pulse through all the cavities avoiding back reflected light. As the optical pulse enters each cavity, it interacts with the respective mechanical resonator. An external signal that perturbs the resonator motion imprints a phase shift φ on the bus field. These shifts accumulate coherently in the input laser pulse, amplifying the effect of the signal. The output pulse is eventually measured to extract information on the phase shift induced by the signal on the mechanical motion.

We model each optomechanical system n as a single optical cavity mode with frequency ω_n that is modulated proportionally to the position $X_n(t)$ of a classical end mirror oscillating with central frequency Ω_n . We assume that all cavity modes are initially in the ground state $|0\rangle$. The signal is assumed to be imprinted on the motion of the end mirrors before the start of the measurement. The dynamics of all light modes (cavity and probe light) is expressed in the reference frame of the (central) frequency of the probe light ω_L . Hence, for each cavity, we have the

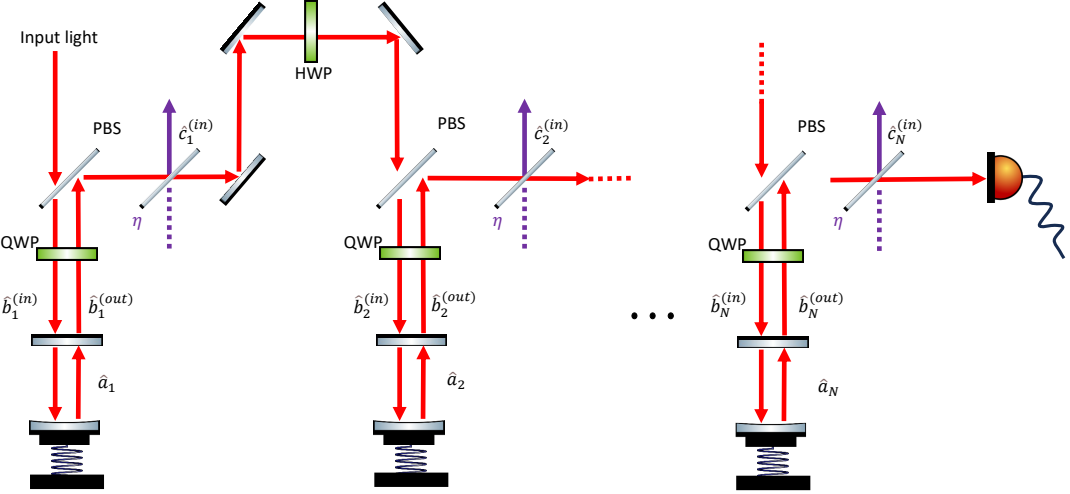


FIG. 1. Sketch of the cascaded system with N optomechanical cavities. An input optical pulse enters the first cavity and, using suitable optical elements (quarter-wave plates (QWPs) and polarizing beam splitters (PBSs)), is directed through all subsequent cavities before reaching the detector. During its propagation, the pulse interacts with each mechanical resonator, acquiring a phase shift that cumulatively encodes the contributions from all N systems.

Hamiltonian

$$\begin{aligned} \hat{H}_n &= \hat{H}_{n,a,0} + \hat{H}_{n,b,0} + \hat{H}_{n,I}, \text{ where} \\ \hat{H}_{n,a,0} &= \hbar(\Delta_n - g_n q_n(t)) \hat{a}_n^\dagger \hat{a}_n, \\ \hat{H}_{n,b,0} &= \hbar \int d\omega (\omega - \omega_L) \hat{b}_n^\dagger(\omega) \hat{b}_n(\omega), \\ \hat{H}_{n,I} &= i\hbar \sqrt{\frac{\kappa_n}{2\pi}} \int d\omega (\hat{b}_n^\dagger(\omega) \hat{a}_n - \hat{b}_n(\omega) \hat{a}_n^\dagger). \end{aligned} \quad (1)$$

$\hat{H}_{n,a,0}$ describes the single-mode field of the n^{th} cavity with detuning $\Delta_n = \omega_n^c - \omega_L$, expressed in terms of bosonic annihilation and creation operators, which satisfy the standard commutation relation $[\hat{a}_n, \hat{a}_n^\dagger] = 1$. The term also contains the shift of the cavity frequency due to the change in position of the mechanical element: the parameter g_n denotes the optomechanical coupling between the mechanical resonator and the cavity field, while $q_n(t) = X_n(t) \sqrt{2m_n \Omega_n / \hbar}$. The second Hamiltonian term $\hat{H}_{n,0,b}$ corresponds to the free Hamiltonian of the outside field, representing a mode continuum in terms of operators $\hat{b}_n^\dagger(\omega)$ and $\hat{b}_n(\omega)$, which satisfy the canonical commutation relations $[\hat{b}_n(\omega), \hat{b}_n^\dagger(\omega')] = \delta(\omega - \omega')$. Finally, the last term $\hat{H}_{n,I}$ models the interaction at the fixed mirror between the cavity and input fields as a beam-splitter with frequency-independent coupling given by the linewidth κ_n (Markovian approximation [35]). This form of the coupling is a good approximation for high-finesse cavities, that is, when the cavity roundtrip time τ_{rt} is much shorter than the time scale of cavity decay (see Chapter 9 of [36]). Therefore, we make the

assumption $\kappa_n \ll 1/\tau_{\text{rt}}$. While many of the following steps are general, eventually, we shall operate in the bad cavity regime in which $\Omega_n \ll \kappa_n$. The optomechanical coupling rates g_n are later also assumed small.

The dynamical degrees of freedom for each cavity are the intra-cavity field \hat{a}_n and the external field $\hat{b}_n(\omega)$. Their dynamics is governed by the Heisenberg equations of motion. Following the standard approach [37] (see Appendix A), we can obtain a formal solution for $\hat{b}_n(\omega, t)$ which we substitute into the equation of motion for $\hat{a}_n(t)$ to obtain the cavity Langevin equation,

$$\partial_t \hat{a}_n(t) = [-\Gamma_n + ig_n q_n(t)] \hat{a}_n(t) - \sqrt{\kappa_n} \hat{b}_n^{(\text{in})}(t), \quad (2)$$

where we used the abbreviation $\Gamma_n = \kappa_n/2 + i\Delta_n$. The input field is defined as

$$\hat{b}_n^{(\text{in})}(t) = \int \frac{d\omega}{\sqrt{2\pi}} e^{-i(\omega - \omega_L)(t - t_0)} \hat{b}_n(\omega, t_0), \quad (3)$$

and $t_0 \rightarrow -\infty$ is the asymptotic initial time at which the cavity and the light field are still decoupled, $[\hat{a}_n(t_0), \hat{b}_n^\dagger(\omega, t_0)] = 0$. With $t_1 \rightarrow \infty$, we can define an analogous expression for the output field,

$$\hat{b}_n^{(\text{out})}(t) = \int \frac{d\omega}{\sqrt{2\pi}} e^{-i(\omega - \omega_L)(t - t_1)} \hat{b}_n(\omega, t_1), \quad (4)$$

where $\hat{b}_n(\omega, t_1)$ is the free field for $t_1 \rightarrow +\infty$, and thereby obtain the input-output relation [37],

$$\hat{b}_n^{(\text{out})}(t) = \hat{b}_n^{(\text{in})}(t) + \sqrt{\kappa_n} \hat{a}_n(t). \quad (5)$$

As the state of the input light field, we consider a Gaussian laser pulse of length τ

$$|\psi(t_0)\rangle = \prod_{\omega} \hat{D}_1 \left[\bar{\beta} \tau e^{-i\omega t_0 - \tau^2(\omega - \omega_L)^2/2} \right] |\text{vac}\rangle, \quad (6)$$

where the continuous wave regime corresponds to $\tau \rightarrow \infty$.

In our cascaded setup, the input field of the n^{th} cavity $\hat{b}_n^{(\text{in})}(t)$ is determined by the output field of the preceding cavity, subject to a propagation delay T . We model possible losses between the cavities by beam-splitter transformations that remove a fraction of the output field and inject an equivalent amount of vacuum noise into the next input field represented by vacuum fields $\hat{c}_n^{(\text{in})}(t)$. This gives rise to the condition

$$\hat{b}_n^{(\text{in})}(t) = \hat{b}_{n-1}^{(\text{out})}(t - T) e^{i\chi} + \hat{c}_{n-1}^{(\text{in})}(t - T) e^{i\xi}, \quad (7)$$

with the abbreviations $\chi = \omega_L T - i \ln \eta$, $\xi = \omega_L T - i \ln \sqrt{1 - \eta^2}$, and the attenuation parameter $\eta \in [0, 1]$. Note that we shift the vacuum fields in time and append a phase for convenience. The above formula applies for $n \geq 2$ as we do not account for extra losses before the first cavity. Iterating (5) and (7), the n -th output field can be expressed in terms of the original first input field, the cumulative response of all n cavities, and the cumulative vacuum noise input,

$$\begin{aligned} \hat{b}_n^{(\text{out})}(t) &= e^{i(n-1)\chi} \left[\hat{b}_1^{(\text{in})}(t - (n-1)T) \right. \\ &\quad \left. + \hat{B}_n(t - (n-1)T) + \hat{C}_n(t - (n-1)T) \right], \end{aligned} \quad (8)$$

introducing the cumulative operators,

$$\begin{aligned} \hat{B}_n(t) &= \sum_{k=1}^n \sqrt{\kappa_k} \hat{a}_k(t + (k-1)T) e^{-i(k-1)\chi}, \\ \hat{C}_n(t) &= e^{i\xi} \sum_{k=1}^{n-1} \hat{c}_k^{(\text{in})}(t + (k-1)T) e^{-ik\chi}. \end{aligned} \quad (9)$$

Ideally, the mechanical signal should coincide with the arrival time of the pulse at the n -th cavity, $(n-1)T$. Let us therefore express the mechanical amplitude as $q_n(t) = Q_n(t - (n-1)T)$, with $Q_n(t)$ ideally centered around $t = 0$. Then, we integrate the cavity Langevin equation (2) for $t > t_0$, make use of the bad cavity regime and let $t_0 \rightarrow -\infty$ to obtain the recursive relation (see Appendix A)

$$\begin{aligned} \hat{B}_n(t) &= \hat{B}_{n-1}(t) - \kappa_n \int_0^\infty dt' e^{-G_n(t)t'} \left[\hat{b}_1^{(\text{in})}(t - t') \right. \\ &\quad \left. + \hat{B}_{n-1}(t - t') + \hat{C}_n(t - t') \right]. \end{aligned} \quad (10)$$

where $\hat{B}_0 \equiv 0$ and $\hat{C}_1 \equiv 0$ and $G_n(t) := \Gamma_n - ig_n Q_n(t)$. We will be mainly concerned with the mean value of

the cumulative response of $N > 1$ cavities, $\langle \hat{B}_N(t) \rangle$, as it is the coherent output field amplitude by which we measure the mechanical signal. When taking the expectation value, the vacuum noise input always vanishes, $\langle \hat{C}_n \rangle = 0$. Therefore, the recursion formula (10) can be formulated in terms of the time-shifted output amplitude, $\beta_n(t) = \beta(t) + \langle \hat{B}_n(t) \rangle$ as

$$\beta_n(t) = \beta_{n-1}(t) - \kappa_n \int_0^\infty dt' e^{-G_n(t)t'} \beta_{n-1}(t - t'), \quad (11)$$

where $\beta_0(t) = \beta(t) := \langle \hat{b}_1^{(\text{in})}(t) \rangle = \bar{\beta} e^{-t^2/2\tau^2}$ and

$$\langle \hat{b}_n^{(\text{out})}(t) \rangle = \eta^{n-1} \beta_n(t - (n-1)T) e^{i(n-1)\omega_L T}. \quad (12)$$

We notice that the attenuation χ does not explicitly appear in the recursion formula (10). The attenuation only enters in the dependence of the actual output field amplitude after n cavities on the β_n in Eq. (12), by the $(n-1)$ -fold attenuation factor.

We denote the Fourier transform of the time-shifted output amplitude as $\tilde{\beta}_n(\omega) = \int dt e^{i\omega t} \beta_n(t) / \sqrt{2\pi}$ and use the inverse Fourier transform to translate the recursion formula (11) into frequency space,

$$\tilde{\beta}_n(\omega) = \tilde{\beta}_{n-1}(\omega) - \frac{\kappa_n}{2\pi} \int d\omega' \tilde{\beta}_{n-1}(\omega') \underbrace{\int dt \frac{e^{i(\omega - \omega')t}}{G_n(t) - i\omega'}}_{=: F_n(\omega', \omega - \omega')}, \quad (13)$$

where $\tilde{\beta}_0(\omega) = \tilde{\beta}(\omega) = e^{i\omega t_0} \langle \hat{b}_1^{(\text{in})}(\omega + \omega_L) \rangle = \bar{\beta} \tau e^{-\tau^2 \omega^2/2}$. As we are concerned with the measurement of weak mechanical signals and realistic optomechanical coupling rates are typically small, $g_n \ll \kappa_n$, we can reasonably expand to lowest order in $|g_n Q_n(t)|/\kappa_n$,

$$F_n(\omega', \Omega) \approx \frac{2\pi\delta(\Omega)}{\Gamma_n - i\omega'} + \frac{\sqrt{2\pi}ig_n \tilde{Q}_n(\Omega)}{(\Gamma_n - i\omega')^2}, \quad (14)$$

where $\tilde{Q}_n(\Omega) = \tilde{q}_n(\Omega) e^{-i\Omega(n-1)T}$ is the Fourier transform of the mechanical displacement. For convenience, we define the integral operator \mathcal{L}_n acting on a frequency-space function by

$$\mathcal{L}_n[\tilde{\alpha}](\omega) := \int d\omega' \left[1 - e^{i\phi_n(\omega')} \right]^2 \tilde{\alpha}(\omega') \frac{\tilde{Q}_n(\omega - \omega')}{\sqrt{2\pi}}, \quad (15)$$

with the cavity response phase $e^{i\phi_n(\omega)} = -(\Gamma_n - i\omega)^*/(\Gamma_n - i\omega)$, i.e., $\phi_n(\omega) = \pi + 2 \arctan(2(\omega - \Delta_n)/\kappa_n)$. The recursion (13) then reads

$$\tilde{\beta}_n = e^{i\phi_n} \tilde{\beta}_{n-1} - i\varepsilon_n \mathcal{L}_n[\tilde{\beta}_{n-1}], \quad \tilde{\beta}_0 = \tilde{\beta}, \quad (16)$$

noting that all $\tilde{\beta}_k$ and ϕ_k are functions of ω and $\varepsilon_n = g_n/\kappa_n$. To first order in ε_n , the consistent solution to

this recursion can be stated as

$$\tilde{\beta}_n \approx e^{i \sum_{j=1}^n \phi_j} \tilde{\beta} - i \sum_{k=1}^n \varepsilon_k e^{i \sum_{j=k+1}^n \phi_j} \mathcal{L}_k \left[e^{i \sum_{\ell=1}^{k-1} \phi_\ell} \tilde{\beta} \right], \quad (17)$$

using the convention $\sum_{n+1}^n (\dots) \equiv 0$. In general, the result cannot be given analytically, but there are two limiting regimes in which approximate analytic treatments are possible: the stroboscopic regime of short light pulses compared to the mechanical signal and the continuous-wave (CW) regime of a light pulse that is much longer than the mechanical signal. The former regime can also be considered beyond the weak-coupling limit (see Appendix A 1).

A. Stroboscopic regime

The stroboscopic regime corresponds to the case of an input pulse that is short compared to the timescale of mechanical motion, $\Omega_n \tau \ll 1$, [38, 39]. This means that not only the average input field but also all the responses $\langle \hat{B}_n(t) \rangle$ and $\beta_n(t)$ remain sharply peaked in time around $t \approx 0$ compared to the mechanical motion. Conversely, in frequency space, the responses $\tilde{\beta}_n$ are spectrally broad compared to the \tilde{Q}_k , and we can therefore approximate $\tilde{\beta}_n(\omega - \Omega) \tilde{Q}_k(\Omega) \approx \tilde{\beta}_n(\omega) \tilde{Q}_k(\Omega)$ for any $n \geq 0$ and $k \geq 1$. In addition, the cavity response times are also assumed short, $\kappa_n \gg \Omega_n$, so that $\phi_n(\omega - \Omega) \tilde{Q}_k(\Omega) \approx \phi_n(\omega) \tilde{Q}_k(\Omega)$. Thus the integral operator (15), applied to such spectrally broad functions, can be approximated by,

$$\mathcal{L}_n[\tilde{\alpha}](\omega) \approx \left[1 - e^{i\phi_n(\omega)} \right]^2 \tilde{\alpha}(\omega) Q_n(0). \quad (18)$$

The 1st-order recursion formula (17) simplifies to,

$$\tilde{\beta}_n(\omega) \approx e^{i \sum_{j=1}^n [\phi_j(\omega) + 2 \frac{g_j}{\kappa_j} Q_j(0) (1 - \cos \phi_j(\omega))]} \tilde{\beta}(\omega). \quad (19)$$

We find that the signals imprint a cumulative spectral phase modulation onto the input field. This result holds, in particular, when the mechanical displacement is constant in time, as the stroboscopic regime then applies for any $\tau < \infty$ and $\kappa > 0$. The $\phi_j(\omega)$ describe the responses of the undisplaced cavities, which filter and reshape light pulses that are spectrally broad compared to the cavity linewidths.

B. Continuous-wave regime

In the opposite regime, the pulse is long compared not only to the cavity lifetime, $\kappa\tau \gg 1$, and the mechanical oscillation, $\Omega_n\tau \gg 1$, but also to the duration of the mechanical signal, $\Omega_n\tau > \Delta\Omega_n\tau \gg 1$. In other words, the light pulse $\tilde{\beta}$ is spectrally much narrower than any of

the ϕ_k and \tilde{Q}_k , so that, whenever the integral operator (15) is applied to a function including $\tilde{\beta}$, one can assume $\omega' \approx 0$ in the arguments of said functions,

$$\mathcal{L}_k[e^{i \sum_\ell \phi_\ell} \tilde{\beta}](\omega) \approx \frac{\kappa_k^2}{\Gamma_k^2} e^{i \sum_\ell \phi_\ell(0)} \tilde{Q}_k(\omega) \beta(0), \quad (20)$$

where the time-domain amplitude $\beta(0) = \int d\omega \tilde{\beta}(\omega) / \sqrt{2\pi}$ arises due to the remaining integral in Eq. (15). The right hand side of Eq. (20) is peaked in frequency space around $\pm\Omega_k$. The delay times T between the cavities can be arbitrary.

Moreover, in Eq. (17), we can also make use of the fact that the \tilde{Q}_k are sharply peaked compared to the cavity linewidths, $\Delta\Omega_k \ll \kappa_n$, and approximate $\phi_n(\omega) \approx \phi_n(0)$ whenever the phases appear together with the \tilde{Q}_k . Hence,

$$\begin{aligned} \tilde{\beta}_n(\omega) &\approx e^{i \sum_{j=1}^n \phi_j(0)} \left[\tilde{\beta}(\omega) \right. \\ &\quad \left. - i\beta(0) \sum_{k=1}^n \frac{g_k \kappa_k}{\Gamma_k^2} e^{-i\phi_k(0)} \tilde{Q}_k(\omega) \right]. \end{aligned} \quad (21)$$

Instead of a cumulative phase imprinted on the broad carrier light pulse in the stroboscopic regime, here we have spectrally resolved sidebands that build up with each cavity and modulate the carrier in time.

C. Continuous-wave regime for continuous signals

There is one more relevant limit that the two discussed regimes do not cover: The light pulse could be long compared to the cavity and the mechanical oscillation frequencies, but the mechanical signals could be perfectly harmonic or quasi-continuous with a longer duration than the light pulse; that is, $\kappa\tau \gg \Omega_n\tau \gg 1 \gg \Delta\Omega_k\tau$. In this case, we make use of the fact that a real-valued oscillating $Q_n(t)$ will yield a Fourier transform $\tilde{Q}_n(\omega)$ that is sharply peaked around $\pm\Omega_n$. This yields spectrally separated sidebands around the carrier $\tilde{\beta}$, which is much less sharply peaked around zero. In (15), we can now reduce the integral to two terms in which we replace the argument of the ϕ_n and of $\tilde{\beta}$ by $\omega' \approx \omega \pm \Omega_k$. Furthermore, we can also approximate $\phi_n(\omega \pm \Omega_k) \approx \phi_n(0)$ as before.

$$\begin{aligned} \mathcal{L}_k[e^{i \sum_\ell \phi_\ell} \tilde{\beta}](\omega) &= \frac{\kappa_n^2}{\Gamma_n^2} e^{i \sum_\ell \phi_\ell(0)} \left[\tilde{\beta}(\omega + \Omega_k) \mathcal{F}_+^{-1}[\tilde{Q}_k](0)^* \right. \\ &\quad \left. + \tilde{\beta}(\omega - \Omega_k) \mathcal{F}_+^{-1}[\tilde{Q}_k](0) \right], \end{aligned} \quad (22)$$

where $\mathcal{F}_+^{-1}[\tilde{Q}_k](0) = \int_0^\infty d\omega' \tilde{Q}_k(\omega') / \sqrt{2\pi}$ is the inverse Fourier transform of $\Theta(\omega) \tilde{Q}_k(\omega)$ at $t = 0$ with Θ the Heaviside step function centered at $\omega = 0$. Plugged into

the solution (17), we obtain a sum of all the sidebands from each cavity

$$\begin{aligned} \tilde{\beta}_n(\omega) \approx & e^{i \sum_{j=1}^n \phi_j(0)} \left[\tilde{\beta}(\omega) \right. \\ & - i \sum_{k=1}^n \frac{g_k \kappa_k}{\Gamma_n^2} e^{-i \phi_k(0)} \left(\tilde{\beta}(\omega + \Omega_k) \mathcal{F}_+^{-1} [\tilde{Q}_k](0)^* \right. \\ & \left. \left. + \tilde{\beta}(\omega - \Omega_k) \mathcal{F}_+^{-1} [\tilde{Q}_k](0) \right) \right]. \end{aligned} \quad (23)$$

In the simplest scenario, the mechanical frequencies are all the same, in which case the sideband amplitudes accumulate. The spectral profile of the sidebands is now given by the $\tilde{\beta}$ -profile, as opposed to (21) where the profile was given by the mechanical signals, \tilde{Q}_n .

III. COHERENT ENHANCEMENT OF METROLOGICAL BOUNDS

Based on the expressions for the output field of the n -th cavity and the cases discussed in the previous section, we now derive achievable lower bounds on the uncertainty with which a signal encoded in the mechanical displacements $Q_n(t)$ can be estimated. We assume that all Q_n are linearly proportional to a single parameter ϑ of the signal. A fundamental upper bound on the signal-to-noise ratio (SNR) for a given setup optimized over all possible measurements can be obtained via the Carmér-Rao bound as $\text{SNR} = \vartheta / \sqrt{\Delta \vartheta} \leq \text{SNR}_{\text{CR}} = \vartheta \sqrt{N \mathcal{H}}$, where N is the number of independent repetitions of the measurement and \mathcal{H} is the Quantum Fisher Information (QFI) [40] associated with the output field after the N -th cavity. Since we consider an initial coherent state of the light field and a quadratic Hamiltonian that preserves Gaussianity, we can restrict our analysis generally to Gaussian states [40, 41]. The key advantage of Gaussian states lies in the fact that they are completely characterized by their first and second moments, collected in the displacement vector $\mathbf{d} = \langle \hat{\mathbf{r}} \rangle^\top$ and the covariance matrix $\boldsymbol{\sigma}$ with components $\sigma_{ij} = \langle \{(\hat{r}_i - d_i), (\hat{r}_j^\dagger - d_j^*)\} \rangle$, respectively. Here, $\hat{\mathbf{r}} = \{\hat{b}_N^{(\text{out})}(\omega_1), \hat{b}_N^{(\text{out})\dagger}(\omega_1), \dots\}$ is the infinite dimensional vector of output creation and annihilation operators of the spectral modes which is obtained from the annihilation operators $\hat{b}_N^{(\text{out})}(t)$ and the corresponding creation operators by Fourier transformation.

This structural property of Gaussian states allows the QFI to be written in a compact form, depending only on the complex covariance matrix and the displacement vector [40, 42]. In our model, the signal parameter is encoded only in the coherent field amplitudes and leaves the second moments unaffected. Therefore, we can restrict our analysis to the corresponding term in the QFI,

$$\mathcal{H}_{\mathbf{d}} = 2(\partial_\vartheta \mathbf{d})^\dagger \boldsymbol{\sigma}^{-1} (\partial_\vartheta \mathbf{d}). \quad (24)$$

The associated Cramér-Rao bound can be saturated by spectrally (or temporally) resolved homodyne detection of the output field. For non-Gaussian field states and homodyne measurements, the CFI of the measured quadrature distribution is lower bounded by the expression (24).

In the following, we assume that the covariance matrix is that of the free field, $\boldsymbol{\sigma} = \mathbb{I}$. The QFI for a continuum of spectral modes reduces to

$$\mathcal{H}_{\mathbf{d}} = 4 \int d\omega |\partial_\vartheta \langle \hat{b}_N^{(\text{out})}(\omega) \rangle|^2 = 4\eta^{N-1} \int d\omega |\partial_\vartheta \tilde{\beta}_N(\omega)|^2. \quad (25)$$

A complete treatment would include perturbations of the covariance matrix due to thermal fluctuations of the mechanical resonator and the back-action of the readout light on the mechanics. In the weak coupling regime ($g_n \gg \kappa_n$), back-action can be safely neglected as the effect on the light field is of second order in g_n . We do not assume that the mechanical elements are cooled to the quantum ground state but consider the opposite regime where the environmental temperature is much larger than $\hbar \Omega_n / k_B$ for all n , where k_B is Boltzmann's constant. Therefore, thermal fluctuations dominate over quantum fluctuations. An analysis of thermal contributions to the covariance matrix is given in Appendix B using the stroboscopic regime as an example.

A. SNR for three limiting cases

We immediately obtain bounds on the SNR after N optomechanical cavities for the different regimes discussed above. We give the expressions for single-shot experiments ($N = 1$) as independent repetitions only give rise to a factor \sqrt{N} . For the stroboscopic regime, we find

$$\begin{aligned} \text{SNR}_{\text{st}}(N) \leq & 2\eta^{\frac{N-1}{2}} \vartheta \left(\int d\omega |\partial_\vartheta \tilde{\beta}_N(\omega)|^2 \right)^{1/2} \\ = & 4\eta^{\frac{N-1}{2}} \left(\int d\omega \left| \sum_{j=1}^N \frac{g_j}{\kappa_j} Q_j(0) \times \right. \right. \\ & \left. \left. \times (1 - \cos \phi_j(\omega)) \tilde{\beta}(\omega) \right|^2 \right)^{1/2}. \end{aligned} \quad (26)$$

In addition, if the pulse spectrum and the cavity detuning are chosen such that the pulse fits into each of the cavity modes, that is, $\tau^{-1}, \Delta_n \ll \kappa_n$, we can evaluate the phases ϕ_j at $\omega = 0$ (the peak of $\tilde{\beta}$), and

$$\text{SNR}_{\text{st}}(N) \leq 4\eta^{\frac{N-1}{2}} N_{\text{in}}^{1/2} \left| \sum_{j=1}^N \frac{g_j}{\kappa_j} Q_j(0) (1 - \cos \phi_j(0)) \right|, \quad (27)$$

where $N_{\text{in}} = \sqrt{\pi}\tau\bar{\beta}^2$ is the number of input photons. We see that the SNR is additive in the case of vanishing noise, $\eta \rightarrow 0$.

In the continuous wave regime with finite signal duration, we obtain

$$\text{SNR}_{\text{cw}}(N) \leq 2\eta^{\frac{N-1}{2}}N_{\text{in}}^{1/2} \frac{1}{\sqrt{\tau\sqrt{\pi}}} \times \left(\int d\omega \left| \sum_{k=1}^N \frac{g_k \kappa_k}{\Gamma_k^2} e^{-i\phi_k(0)} \tilde{Q}_k(\omega) \right|^2 \right)^{1/2} \quad (28)$$

If the spectral sidebands produced by each optomechanical cavity are assumed to be equivalent up to their amplitude, that is, $\tilde{Q}_k(\omega) = \tilde{Q}_{k,0}\tilde{S}(\omega)$, the integration over $|\tilde{S}(\omega)|^2$ can be performed independently from the sum over cavities. This results in

$$\text{SNR}(N) \leq 2\eta^{\frac{N-1}{2}}N_{\text{in}}^{1/2} \mathcal{M}_{\text{sb}} \left| \sum_{k=1}^N \frac{g_k \kappa_k}{\Gamma_k^2} e^{-i\phi_k(0)} \tilde{Q}_{k,0} \right| \quad (29)$$

where $\mathcal{M}_{\text{sb}} = (\int d\omega |\tilde{S}(\omega)|^2)^{1/2} / \sqrt{\tau\sqrt{\pi}}$. For the case of a continuous signal, we use Eq. (23) and take into account that the two sidebands do not overlap (since $\Omega_k\tau \gg 1$) to obtain

$$\text{SNR}(N) \leq 2\eta^{\frac{N-1}{2}}N_{\text{in}}^{1/2} \times \left(\left| \sum_{k=1}^N \frac{g_k \kappa_k}{\Gamma_k^2} e^{-i\phi_k(0)} \mathcal{F}_+^{-1}[\tilde{Q}_k](0)^* \right|^2 + \left| \sum_{k=1}^N \frac{g_k \kappa_k}{\Gamma_k^2} e^{-i\phi_k(0)} \mathcal{F}_+^{-1}[\tilde{Q}_k](0) \right|^2 \right)^{1/2} \quad (30)$$

This concludes the limiting cases that we treat in this article. In the following we restrict our considerations to equal cavities which leads to general results that apply to all limiting cases.

B. Equal cavities

If we assume that all sensors provide the same contribution to the SNR, we obtain the upper bound for the SNR after N sensors as

$$\text{SNR}_{\text{CR}}(N) = N\eta^{\frac{N-1}{2}} \text{SNR}_{\text{CR}}(1) \quad (31)$$

for all three cases, where $\text{SNR}_{\text{CR}}(1)$ is the bound of the SNR for a single optomechanical cavity. To evaluate the advantage of the cascaded sensing scheme in comparison to incoherent combination of the measurement outcomes of N optomechanical sensors into one measurement statistics, we have to compare the SNR scaling above with the scaling of independent measurements

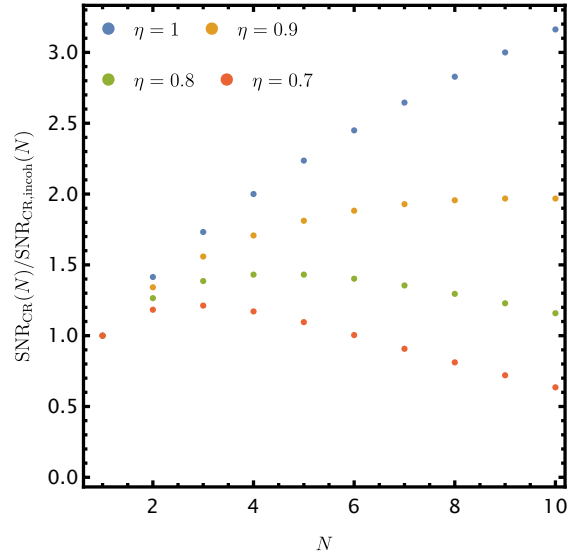


FIG. 2. Plot of the ratio of the upper bounds for the coherent and incoherent signal to noise ratios $\text{SNR}_{\text{CR}}(N)$ and $\text{SNR}_{\text{CR,incoh}}(N)$. In the ideal case of no losses (blue dots) the ratio increases indefinitely proportionally to \sqrt{N} . As losses are introduced (yellow dots $\eta = 0.9$, green dots $\eta = 0.8$, red dots $\eta = 0.7$) there is an interplay between the coherent accumulation of the signal and decoherence which leads to an optimal number of systems N_{opt} above which the advantage is lost, and the SNR decreases. Higher values of losses correspond to lower SNR-ratios and smaller N_{opt} .

$\text{SNR}_{\text{CR,incoh}}(N) = \sqrt{N}\text{SNR}_{\text{CR}}(1)$. In Fig. 2, the quotient $\text{SNR}_{\text{CR}}(N)/\text{SNR}_{\text{CR,incoh}}(N) = \sqrt{N}\eta^{(N-1)/2}$ is plotted as function of N for different values of η . While the SNR increases indefinitely with N for attenuation parameter $\eta = 1$, for each $\eta \neq 1$, there exists an N_{opt} at which $\text{SNR}_{\text{CR}}(N)/\text{SNR}_{\text{CR,incoh}}(N)$ reaches a maximum. Without any further noise sources and assuming that measurements are implemented that actually saturate the bound (e.g. homodyning ones), N_{opt} is the number of optomechanical cavities to optimally exploit the cascaded sensing scheme. It is easy to show analytically that N_{opt} is one of the two integers that are closest to $-\log(\eta)^{-1}$. For η very close to 1 (roughly for values larger 0.7), we find that N_{opt} is the integer part of $\eta/(1-\eta)$ and $\text{SNR}_{\text{CR}}(N_{\text{opt}})/\text{SNR}_{\text{CR,incoh}}(N_{\text{opt}}) \approx 1/\sqrt{e(1-\eta)}$, where e is Euler's number.

In Fig. 3, we show plots of the optimal number of sensors N_{opt} and the corresponding enhancement ratio $\text{SNR}_{\text{CR}}(N_{\text{opt}})/\text{SNR}_{\text{CR,incoh}}(N_{\text{opt}})$ for values of η between 0.8 and 0.999.

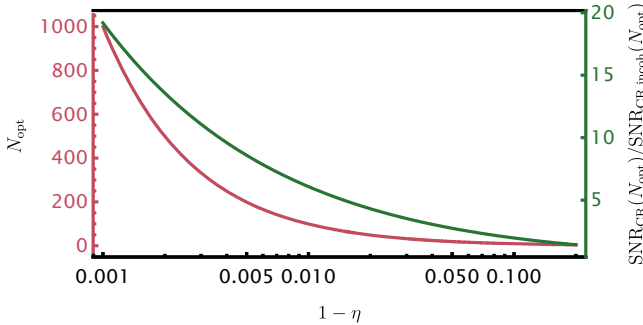


FIG. 3. Plots of the optimal number of sensors N_{opt} and the maximal SNR ratio $\text{SNR}_{\text{CR}}(N_{\text{opt}})/\text{SNR}_{\text{CR,incoh}}(N_{\text{opt}})$ as a function of the loss from the light field between the sensors $1 - \eta$ from $\eta = 0.999$ to $\eta = 0.8$.

IV. POTENTIAL APPLICATIONS

In this section, we discuss three sensing applications which could profit from the cascaded sensing scheme presented in this article.

A. Dark Matter

Despite the abundance of astrophysical and cosmological observations in favor of the existence of Dark Matter (DM) particles, the fundamental nature of these constituents has not been identified. DM is expected to interact very weakly with standard matter (SM) and perhaps only through gravity. A crucial characteristic such as the mass has not been established yet, and the range of possible values is very broad, from 10^{-58} kg up to several of solar masses. Observations indicate that the local dark matter (DM) mass density is $\rho_\chi \simeq 5.3 \times 10^{-22}$ kg/m³ [20]. DM candidates are usually classified according to their masses m_χ into two main categories and their interaction with standard matter can be described in different ways: heavy DM or particle-like candidates defined by $m_\chi > 10^{-36}$ kg are expected to behave as a dilute gas of single particles; ultralight wave-like candidates, with 10^{-58} kg < $m_\chi < 0.1 \times 10^{-36}$ kg are described as a persistent wave-like field. Different experimental setups and measurement apparatus are required to investigate different parts of the parameter space. However, for all the models interacting with SM only through mass, massive mechanical sensors are required, and optomechanics offer potential platforms to search a wide range of candidates. Assuming that the DM is in equilibrium with the galaxy halo, it is expected to move at a typical speed of $v_\chi \sim 10^5$ m/s, from the viral theorem, and then having a de Broglie wavelength of $\lambda_\chi = 2\pi\hbar/(m_\chi v_\chi)$ [4]. We focus on “ultra light” DM, where candidates possess low mass ($m_\chi < 0.1 \times 10^{-36}$ kg) and extremely large

mode occupation numbers. This means that we can treat these candidates as a bosonic field that oscillates in time with wavelength $\lambda_\chi > 1$ mm and natural field frequency $\omega_\chi = m_\chi c^2/\hbar \lesssim 2\pi \times 10^{13}$ s⁻¹. The frequency spread $\delta\omega_\chi \approx m_\chi v_\chi^2/(2\hbar) \approx 2\pi \times 10^6$ s⁻¹ leads to a coherence time $T_{\text{coh}} \approx 2\pi/\delta\omega_\chi \approx 2\pi \times 10^7/\omega_\chi$ [20]. These models therefore give rise to extremely weak, coherent and persistent field oscillations that can potentially be detected, and the core problem reduces to the detection of a weak signal which makes it an extremely suitable application for the cascaded optomechanical scheme. Assuming that DM consists of a single ultralight field, the observable signature is a temporally oscillating force that acts on the detector, with strength proportional to the mass. This can be parametrised as

$$F_\chi = g_\chi \rho_\chi f(t), \quad (32)$$

where g_χ is the unknown DM coupling that depends on the DM model assumed, ρ_χ is the local DM density, and $f(t)$ contains the time-dependence of the signal. In the steady state at resonance, the resulting amplitude of a mechanical sensor with frequency Ω and damping rate $\Omega\zeta$ is $q_{\chi,s} = F_\chi/(2m\Omega^2\zeta)$. Hence, a search for DM could be done by trying to estimate the parameter $\vartheta_\chi = g_\chi \rho_\chi$ by optomechanical read-out of the mechanical amplitude. This approach is promising, as it is supported by several studies on optomechanical methods for DM detection [19–21, 43, 44]. Since some sensors are small systems, it has also been already proposed to use arrays of many of these sensors [20]. Due to the small size of the systems and the possibility to combine them with integrated optics, losses between sensors may be significantly restricted. In that case, our framework of cascaded optomechanical sensing is applicable and the coherent enhancement of sensitivity provides a factor \sqrt{N} in the most ideal case.

B. Gravitational waves

Since the first detection of gravitational waves by the LIGO/Virgo collaboration [45], many more transient signals from binary mergers have been observed and gravitational astrophysics is expanding quickly with new detectors going online and being proposed. Also continuous gravitational wave signals from large binaries in the low frequency regime are very likely to be detected soon with LISA in space [46]. However, signals from binary mergers only represent a subset of possible signals. Other types include non-transient gravitational wave signals in the kHz-band and above that can be continuous, for example, emitted by fast rotating neutron stars [47–49], or a stochastic background, for example, emitted during the rapid evaporation of primordial black holes [50].

Besides the general possibility to employ interferometric gravitational wave antennas like LIGO and Virgo

for the detection of non-transient gravitational wave signals [48, 50], there are several other proposals to employ highly controlled mechanical sensors for the detection of continuous gravitational wave signals at frequencies in the kHz range and above [22, 51–55]. Since these sensors are usually much smaller than the wavelength of the gravitational waves they are proposed to detect, in essence, a gravitational wave of frequency ω and strain h acts as a time dependent tidal force with gradient [56, 57]

$$|\nabla F_h| \propto \omega^2 h/2. \quad (33)$$

In many cases, the proposed readout mechanism for the mechanical sensors is via the electromagnetic field and sensors can be bundled into a larger volume to form a more sensitive detector network (as has been demonstrated for torsion bar antennas [58] and interferometers [59]). Therefore, gravitational wave detection of continuous high-frequency signals is another potential application for cascaded optomechanical metrology.

C. Gravitational field of ultra-relativistic matter

A third potential application of the cascaded optomechanical sensing scheme is the detection of the gravitational field of ultra-relativistic matter at the Large Hadron Collider (LHC) [60]. The gravitational attraction of the circulating proton bunches is dominated by their kinetic energy which is a factor ~ 7000 larger than the energy associated with their rest mass. While the gravitational effect of kinetic energy is evidenced in many astrophysical observations, this prediction of general relativity has not been experimentally tested. Tests at the LHC would enable full control over the generation of ultra-relativistic sources of gravitational fields, allowing for precise and repeatable measurements [61]. Besides the exciting possibility of the first direct evidence for the gravitational attraction of kinetic energy, gravity measurements at particle accelerators could also be used to test alternative gravity theories in yet unexplored regimes [62]. The LHC consists of a 27 km ring in which 2800 bunches of protons circulate at speeds approaching c , with each bunch carrying a total energy of 10^5 J distributed among approximately 1.15×10^{11} protons. Each bunch is approximately 30 cm long and lasts approximately 1 ns. To profit from phase locking techniques, a sensor positioned near the ring must resonate at frequencies matching the bunch passage rate: the full beam provides a rate of 31.2 MHz, while a single bunch orbiting the ring passes with a frequency of 11 kHz. Lower frequencies can be achieved through periodic modulation of the beam position, where the LHC beam is active for half the sensor's oscillation period. One can estimate the effective acceleration amplitude driving the sensor as [60]

$$a_{0,\text{LHC}} \sim \frac{4GP}{c^2 d}, \quad (34)$$

where G is the gravitational constant, P the average power of the particle beam (3.8×10^{12} W in the case of the LHC) and d the distance between the center of the mechanical resonator and the beam axis. This leads to the corresponding steady state oscillation amplitude $q_{\chi,s} = a_{\text{LHC}}/(2\Omega^2\zeta)$ of the mechanical resonator.

Since the proton bunches at the LHC move in a 27 km long ring, in principle, many acceleration sensors can be placed around the beam line and their signals can be correlated. Therefore, significant enhancement could be provided by the cascaded sensing scheme if losses between sensors can be limited.

V. CONCLUSIONS

We have shown that coherently coupling N optomechanical sensors via their output light field in a cascaded way can improve the total signal-to-noise ratio (SNR) significantly. In the ideal case, that is, without loss from the output light field between the cavities, this version of coherent averaging leads to an increase of the SNR proportional to N while incoherent averaging leads to the usual scaling with \sqrt{N} . If losses are included, represented by an attenuation factor η , the advantage of the cascaded readout over the incoherent readout scales as $\eta^{(N-1)/2}\sqrt{N}$ which implies an optimal value for N beyond which the advantage starts to decrease. For η close to one, the enhancement factor is approximately $1/\sqrt{e\eta}$, where e is Eulers number, which can mean a significant improvement.

We have discussed that the cascaded sensing scheme can be employed in fundamental research with the examples of dark matter detection, gravitational wave astronomy and measurements of the gravitational field of ultra-relativistic matter. We expect that further proposals for applications may be found in the future.

In this work we modeled the mechanical oscillator as a moving end mirror of a cavity without considering back-action from the readout light. While this is justified for the case of macroscopic mirrors and small back-action (as we show in the appendix), it may be worthwhile to extend our analysis to a full quantum mechanical model treating the mirror position as another dynamical degree of freedom. This is left for future work.

Acknowledgements

We thank Germain Tobar, Navdeep Arya, Magdalena Zych, Teodor Strömberg and Onur Hosten for useful discussions. MMM acknowledges support from the Walter Benjamin Programme (project number 510053905) and from the Austrian Science Fund (FWF) [10.55776/COE1]. DB acknowledges funding by the EU

EIC Pathfinder project QuCoM (101046973). D.R. acknowledges funding by the Federal Ministry of Education and Research of Germany in the project “Open6GHub” (grant number: 16KISK016), financial support from EPSRC (Engineering & Physical Sciences Research Coun-

cil, United Kingdom) Grant Number EP/X009467/1, and support by the Deutsche Forschungsgemeinschaft (DFG, German Research Foundation) under Germany’s Excellence Strategy – EXC-2123 QuantumFrontiers – 390837967.

APPENDIX

Appendix A: General recursion formula

We begin from the Hamiltonian \hat{H}_n describing each one-sided cavity, written in a frame rotating at the (central) probe frequency ω_L . Equivalently, one may transform into the frame co-rotating with the input light by applying the unitary $\hat{U}_n(t) = \exp\{i\omega_L[\hat{a}_n^\dagger \hat{a}_n + \int d\omega \hat{b}_n^\dagger(\omega) \hat{b}_n(\omega)]t\}$. In this frame, the bare cavity resonance ω_n appears through the detuning $\Delta_n = \omega_n - \omega_L$ and the linewidth κ_n . The mechanical signal is treated classically and encoded in the dimensionless quadrature $q_n(t)$, oscillating at a mechanical frequency Ω_n . We work in the bad-cavity limit $\Omega_n \ll \kappa_n$, and assume weak optomechanical coupling strengths g_n .

The equations of motion for the co-rotating field operators read

$$\begin{aligned}\partial_t \hat{a}_n(t) &= -i\Delta_n \hat{a}_n(t) + ig_n q_n(t) \hat{a}_n(t) - \sqrt{\frac{\kappa_n}{2\pi}} \int d\omega \hat{b}_n(\omega, t), \\ \partial_t \hat{b}_n(\omega, t) &= \sqrt{\frac{\kappa_n}{2\pi}} \hat{a}_n(t) - i(\omega - \omega_L) \hat{b}_n(\omega, t),\end{aligned}\quad (\text{A1})$$

where $t_0 \rightarrow -\infty$ denotes the asymptotic initial time at which the cavity and the external field are uncoupled, so that $[\hat{a}_n(t_0), \hat{b}_n^\dagger(\omega, t_0)] = 0$. The continuum of operators outside the cavity satisfies the standard commutation relations $[\hat{b}_n(\omega, t), \hat{b}_n^\dagger(\omega', t)] = \delta(\omega - \omega')$ at all times. Under the Markov approximation of a flat coupling density, one can integrate the second equation from t_0 to t and substitute the result into the first equation, yielding

$$\partial_t \hat{a}_n(t) = \left[-i\Delta_n - \frac{\kappa_n}{2} + ig_n q_n(t) \right] \hat{a}_n(t) - \sqrt{\kappa_n} \hat{b}_n^{(\text{in})}(t), \quad \hat{b}_n^{(\text{in})}(t) = \int \frac{d\omega}{\sqrt{2\pi}} e^{-i(\omega - \omega_L)(t - t_0)} \hat{b}_n(\omega, t_0). \quad (\text{A2})$$

Alternatively, the cavity dynamics may be written in terms of the output field $\hat{b}_n^{(\text{out})}(t) = (2\pi)^{-1/2} \int d\omega e^{-i(\omega - \omega_L)(t - t_1)} \hat{b}_n(\omega, t_1)$ with $t_1 \rightarrow \infty$, leading to the usual input–output relation [37]

$$\hat{b}_n^{(\text{out})}(t) = \hat{b}_n^{(\text{in})}(t) + \sqrt{\kappa_n} \hat{a}_n(t). \quad (\text{A3})$$

The corresponding Heisenberg-picture operators in the laboratory frame are $\hat{a}_n^{(\text{H})}(t) = \hat{a}_n(t) e^{-i\omega_L t}$ and $\hat{b}_n^{(\text{H})}(\omega, t) = \hat{b}_n(\omega, t) e^{-i\omega_L t}$. This representation is useful when evaluating expectation values with respect to the initial state of the incoming field before the first cavity,

$$|\psi(t_0)\rangle = \prod_{\omega} \hat{D}_1 \left[\beta_0 \tau e^{-i\omega t_0 - \tau^2(\omega - \omega_L)^2/2} \right] |\text{vac}\rangle, \quad (\text{A4})$$

which corresponds to a Gaussian pulse of duration τ , centered at ω_L , and arriving at the first cavity at $t = 0$. One then finds

$$\langle \hat{b}_1^{(\text{in}, \text{H})}(t) \rangle = \int \frac{d\omega}{\sqrt{2\pi}} e^{-i\omega(t - t_0)} \langle \psi(t_0) | \hat{b}_1^{(\text{H})}(\omega, t_0) | \psi(t_0) \rangle = \beta_0 e^{-t^2/2\tau^2 - i\omega_L t}, \quad \text{so that } \beta(t) := \langle \hat{b}_1^{(\text{in})}(t) \rangle = \beta_0 e^{-t^2/2\tau^2}. \quad (\text{A5})$$

The continuous-wave limit is recovered by taking $\tau \rightarrow \infty$.

In the cascaded configuration, the asymptotic output of cavity $(n-1)$ serves as the input to cavity n after free propagation over a delay time $T \gg 1/\kappa$. In the laboratory frame this implies $\hat{b}_n^{(\text{in}, \text{H})}(t) = \hat{b}_{n-1}^{(\text{out}, \text{H})}(t - T)$, and in the co-rotating frame,

$$\hat{b}_n^{(\text{in})}(t) = \hat{b}_{n-1}^{(\text{out})}(t - T) e^{i\omega_L T}, \quad n > 1. \quad (\text{A6})$$

By repeatedly applying Eqs. (A3) and (A6), the output field of the n th cavity can be written in terms of the original input field and the accumulated response of all preceding cavities,

$$\hat{b}_n^{(\text{out})}(t) = \hat{b}_{n-1}^{(\text{out})}(t-T)e^{i\omega_L T} + \sqrt{\kappa_n} \hat{a}_n(t) = \dots = \hat{b}_1^{(\text{in})}(t-(n-1)T)e^{i(n-1)\omega_L T} + \underbrace{\sum_{j=0}^{n-1} \sqrt{\kappa_{n-j}} \hat{a}_{n-j}(t-jT)e^{ij\omega_L T}}_{= \hat{B}_n(t-(n-1)T)e^{i(n-1)\omega_L T}}. \quad (\text{A7})$$

The cumulative response up to cavity n is therefore defined as

$$\hat{B}_n(t) = \sum_{j=0}^{n-1} \sqrt{\kappa_{n-j}} \hat{a}_{n-j}(t+(n-j-1)T)e^{-i(n-j-1)\omega_L T} = \sum_{k=1}^n \sqrt{\kappa_k} \hat{a}_k(t+(k-1)T)e^{-i(k-1)\omega_L T}. \quad (\text{A8})$$

Ideally, the mechanical modulation should be synchronized with the arrival of the pulse at the n th cavity $(n-1)T$. We therefore write $q_n(t) = Q_n(t-(n-1)T)$, with $Q_n(t)$ centered around $t=0$. Introducing $\Gamma_n = \kappa_n/2 + i\Delta_n$, we integrate the Langevin equation (A2) to obtain

$$\begin{aligned} \hat{a}_n(t) &= \hat{a}_n(t_0) \exp \left[-\Gamma_n(t-t_0) + ig_n \int_{t_0}^t dt' Q_n(t'-(n-1)T) \right] \\ &\quad - \sqrt{\kappa_n} \int_{t_0}^t dt' \hat{b}_n^{(\text{in})}(t') \exp \left[-\Gamma_n(t-t') + ig_n \int_{t'}^t dt'' Q_n(t''-(n-1)T) \right] \\ &\approx \hat{a}_n(t_0) e^{-G_n(t-(n-1)T)(t-t_0)} - \sqrt{\kappa_n} \int_0^{t-t_0} dt' \hat{b}_n^{(\text{in})}(t-t') e^{-G_n(t-(n-1)T)t'}, \quad \text{with } G_n(t) := \Gamma_n - ig_n Q_n(t). \end{aligned} \quad (\text{A9})$$

In the approximation, we have used the bad-cavity condition: $Q_n(t') \approx Q_n(t)$ as long as t' lies within the response time of the cavity, $|t-t'| \lesssim 1/\kappa_n$.

Next, we shift the time argument by the pulse arrival time and rewrite the result in terms of the first input field and the cumulative response of the earlier cavities,

$$\begin{aligned} \hat{a}_n(t+(n-1)T) &= \hat{a}_n(t_0) e^{-G_n(t)(t+(n-1)T-t_0)} - \sqrt{\kappa_n} \int_0^{t+(n-1)T-t_0} dt' \hat{b}_{n-1}^{(\text{out})}(t+(n-2)T-t') e^{-G_n(t)t'+i\omega_L T} \\ &= \hat{a}_n(t_0) e^{-G_n(t)(t+(n-1)T-t_0)} - \sqrt{\kappa_n} \int_0^{t+(n-1)T-t_0} dt' e^{-G_n(t)t'+i(n-1)\omega_L T} \left[\hat{b}_1^{(\text{in})}(t-t') + \hat{B}_{n-1}(t-t') \right] \\ &\xrightarrow{t_0 \rightarrow -\infty} -\sqrt{\kappa_n} e^{i(n-1)\omega_L T} \int_0^\infty dt' e^{-G_n(t)t'} \left[\hat{b}_1^{(\text{in})}(t-t') + \hat{B}_{n-1}(t-t') \right] \quad \text{for any finite } t. \end{aligned} \quad (\text{A10})$$

This limit is justified as long as the cavity field is evaluated at finite times, well after the asymptotic past t_0 .

To derive a recursion relation for \hat{B}_n , we sum according to Eq. (A8),

$$\begin{aligned} \hat{B}_n(t) &= - \sum_{k=1}^n \kappa_k \int_0^\infty dt' e^{-G_k(t)t'} \left[\hat{b}_1^{(\text{in})}(t-t') + \hat{B}_{k-1}(t-t') \right] \\ &= -\kappa_n \int_0^\infty dt' e^{-G_n(t)t'} \left[\hat{b}_1^{(\text{in})}(t-t') + \hat{B}_{n-1}(t-t') \right] - \underbrace{\sum_{k=1}^{n-1} \kappa_k (\dots)}_{= \hat{B}_{n-1}(t)} \\ &= \hat{B}_{n-1}(t) - \kappa_n \int_0^\infty dt' e^{-G_n(t)t'} \left[\hat{b}_1^{(\text{in})}(t-t') + \hat{B}_{n-1}(t-t') \right]. \end{aligned} \quad (\text{A11})$$

With $\hat{B}_0 \equiv 0$, this recursion holds for any $n \geq 1$. Because of the explicit time dependence in the exponential, the integral does not reduce to a simple convolution, and in general no closed-form analytic solution is expected.

Our main interest lies in the expectation value of the cumulative response of a large number $N \gg 1$ of cavities, $\langle \hat{B}_N(t) \rangle$, as it is the coherent output field amplitude by which we measure the mechanical signal. It is convenient to introduce the time-shifted output amplitude $\beta_n(t) = \beta(t) + \langle \hat{B}_n(t) \rangle$, for which the recursion becomes

$$\langle \hat{b}_n^{(\text{out})}(t) \rangle = \beta_n(t-(n-1)T)e^{i(n-1)\omega_L T} \quad \Rightarrow \quad \beta_n(t) = \beta_{n-1}(t) - \kappa_n \int_0^\infty dt' e^{-G_n(t)t'} \beta_{n-1}(t-t'), \quad (\text{A12})$$

with $\beta_0 \equiv \beta$. The measured output in the laboratory frame and its Fourier components are given by

$$\langle \hat{b}_n^{(\text{out},\text{H})}(t) \rangle = \beta_n(t - (n-1)T) e^{i\omega_L[(n-1)T-t]}, \quad \langle \hat{b}_n^{(\text{out},\text{H})}(\omega) \rangle = \int \frac{dt}{\sqrt{2\pi}} e^{i\omega t} \langle \hat{b}_n^{(\text{out},\text{H})}(t) \rangle = \tilde{\beta}_n(\omega - \omega_L) e^{i(n-1)\omega T}. \quad (\text{A13})$$

Here $\tilde{\beta}_n(\omega) = \int dt e^{i\omega t} \beta_n(t) / \sqrt{2\pi}$. Using the inverse Fourier transform, Eq. (A12) can be expressed in frequency space as

$$\begin{aligned} \tilde{\beta}_n(\omega) &= \tilde{\beta}_{n-1}(\omega) - \kappa_n \int \frac{dt}{\sqrt{2\pi}} e^{i\omega t} \int_0^\infty dt' e^{-G_n(t)t'} \int \frac{d\omega'}{\sqrt{2\pi}} e^{-i\omega'(t-t')} \tilde{\beta}_{n-1}(\omega') \\ &= \tilde{\beta}_{n-1}(\omega) - \frac{\kappa_n}{2\pi} \int d\omega' \tilde{\beta}_{n-1}(\omega') \underbrace{\int dt \frac{e^{i(\omega-\omega')t}}{G_n(t) - i\omega'}}_{=:F_n(\omega', \omega - \omega')} . \end{aligned} \quad (\text{A14})$$

Since realistic optomechanical couplings satisfy $g_n \ll \kappa_n$, and we are interested in weak mechanical signals, it is natural to expand to lowest order in $|g_n Q_n(t)|/\kappa_n$,

$$F_n(\omega', \Omega) \approx \frac{2\pi\delta(\Omega)}{\Gamma_n - i\omega'} + \frac{\sqrt{2\pi}ig_n\tilde{Q}_n(\Omega)}{(\Gamma_n - i\omega')^2}, \quad \text{with} \quad \tilde{Q}_n(\Omega) = \int \frac{dt}{\sqrt{2\pi}} Q_n(t) e^{i\Omega t} = \tilde{q}_n(\Omega) e^{-i\Omega(n-1)T}. \quad (\text{A15})$$

This first-order expansion is sufficient to evaluate the quantum Fisher information around vanishing mechanical signal amplitude.

The mechanical excitation oscillates at a frequency $\Omega_n \ll \kappa_n$, but it need not be strictly harmonic. One may instead consider a mechanical pulse with spectral profile $\tilde{Q}_n(\Omega)$ centered at Ω_n and width $\Delta\Omega_n < \Omega_n$. Introducing the cavity phase response $e^{i\phi_n(\omega)} = -(\Gamma_n - i\omega)^*/(\Gamma_n - i\omega)$, the recursion becomes

$$\tilde{\beta}_n(\omega) = e^{i\phi_n(\omega)} \tilde{\beta}_{n-1}(\omega) - i \frac{\kappa_n g_n}{\sqrt{2\pi}} \int d\omega' \frac{\tilde{\beta}_{n-1}(\omega')}{(\Gamma_n - i\omega')^2} \tilde{Q}_n(\omega - \omega') + \mathcal{O}\{\varepsilon_n^2\}, \quad \tilde{\beta}_0(\omega) = \tilde{\beta}(\omega). \quad (\text{A16})$$

The integral term is of order $\varepsilon_n := g_n/\kappa_n$ and represents a convolution in frequency, with a width determined by the broader of the two integrands. Iterating this relation while consistently retaining only first-order terms in ε_n yields the total response.

For compactness, we define the linear operator \mathcal{L}_n acting on a frequency-domain function as

$$\mathcal{L}_n[\tilde{\alpha}](\omega) := \int d\omega' \frac{\kappa_n^2 \tilde{\alpha}(\omega')}{(\Gamma_n - i\omega')^2} \frac{\tilde{Q}_n(\omega - \omega')}{\sqrt{2\pi}} = \int d\omega' \left[1 - e^{i\phi_n(\omega')} \right]^2 \tilde{\alpha}(\omega') \frac{\tilde{Q}_n(\omega - \omega')}{\sqrt{2\pi}}. \quad (\text{A17})$$

In this notation, the recursion reads

$$\tilde{\beta}_n = e^{i\phi_n} \tilde{\beta}_{n-1} - i\varepsilon_n \mathcal{L}_n[\tilde{\beta}_{n-1}], \quad \tilde{\beta}_0 = \tilde{\beta}, \quad (\text{A18})$$

where $\tilde{\beta}_k$ and ϕ_k are functions of ω . The consistent first-order solution is

$$\tilde{\beta}_n = \exp \left\{ i \sum_{j=1}^n \phi_j \right\} \tilde{\beta} - i \sum_{k=1}^n \varepsilon_k \exp \left\{ i \sum_{j=k+1}^n \phi_j \right\} \mathcal{L}_k \left[\exp \left\{ i \sum_{\ell=1}^{k-1} \phi_\ell \right\} \tilde{\beta} \right] + \sum_{j,k} \mathcal{O}\{\varepsilon_j \varepsilon_k\}, \quad (\text{A19})$$

which follows directly by induction, with the convention $\sum_{n+1}^n (\dots) \equiv 0$.

1. Stroboscopic regime beyond weak signals

The stroboscopic regime also applies when the optomechanical coupling or mechanical signal is not weak. In this case, let us directly approximate $G_n(t) \approx G_n(0)$ in the time-domain recursion formula (A12),

$$\beta_n(t) \approx \beta_{n-1}(t) - \kappa_n \int_{-\infty}^\infty dt' \Theta(t') e^{-G_n(0)t'} \beta_{n-1}(t - t'), \quad (\text{A20})$$

with Θ is the Heaviside function. Now we have a convolution that is conveniently solved in Fourier space. To this end, we introduce the Fourier transform of the convolution kernel and an associated signal phase,

$$\begin{aligned} S_n(\omega) &= \int dt \Theta(t) e^{-G_n(0)t+i\omega t} = \frac{1}{G_n(0) - i\omega} = \frac{1}{\Gamma_n - i[g_n Q_n(0) + \omega]}, \\ 1 - \kappa_n S_n(\omega) &= -\frac{\Gamma_n^* + i[g_n Q_n(0) + \omega]}{\Gamma_n - i[g_n Q_n(0) + \omega]} = -\frac{S_n(\omega)}{S_n^*(\omega)} =: e^{i\chi_n(\omega)}, \end{aligned} \quad (\text{A21})$$

$$\tilde{\beta}_n(\omega) = \tilde{\beta}_{n-1}(\omega) - \kappa_n S_n(\omega) \tilde{\beta}_{n-1}(\omega) = e^{i\chi_n(\omega)} \tilde{\beta}_{n-1}(\omega) = \exp \left\{ i \sum_{k=1}^n \chi_k(\omega) \right\} \tilde{\beta}(\omega). \quad (\text{A22})$$

We also see an accumulating phase in the output spectral amplitude as the signature of coherent averaging.

Appendix B: Thermal noise

Inclusion of thermal and quantum back action noise requires a full quantum treatment, since, these two noise contributions arise when also the mechanical degree of freedom is treated as a quantum operator.

The aim of this appendix is to show that both effects can be neglected under reasonable conditions. We restrict our considerations to the stroboscopic regime where the light pulse is much shorter than the mechanical period ($\tau^{-1} \gg \Omega$) while we still assume that it is much longer than the cavity decay time ($\kappa \gg \tau^{-1}$). Furthermore, we only consider the interaction of the light pulse with a single cavity. This is reasonable since if we find that the contribution is small, then it can be added up linearly for many cavities. Starting with the Hamiltonian in Eq. (1), we can drop the index n , and we need to add the free Hamiltonian for the mechanical oscillator $\hat{H}_M = \hbar\Omega\hat{c}^\dagger\hat{c}$, where \hat{c}^\dagger and \hat{c} are the creation and annihilation operator for the mechanical mode. The equations of motion are

$$\left\{ \begin{array}{l} \partial_t \hat{c}(t) = -i\Omega \hat{c}(t) + i \frac{g}{\sqrt{2}} \hat{a}^\dagger(t) \hat{a}(t), \\ \partial_t \hat{a}(t) = -i\Delta \hat{a}(t) + i \frac{g}{\sqrt{2}} \hat{a}(t) (\hat{c}^\dagger(t) + \hat{c}(t)) - \sqrt{\frac{\kappa}{2\pi}} \int d\omega \hat{b}(\omega, t), \\ \partial_t \hat{b}(\omega, t) = -i(\omega - \omega_L) \hat{b}(\omega, t) + \sqrt{\frac{\kappa}{2\pi}} \hat{a}(t). \end{array} \right. \quad (\text{B1})$$

We assume that the resonator is initially in a thermal state at temperature T , which is then coherently displaced by the signal we aim to detect. For simplicity, we also assume that the thermalisation time is long compared to the probing time and the resonator state is thus given by a displaced thermal state oscillating at the mechanical frequency Ω . What we measure is the modulation of the coherent output light amplitude due to this oscillation for a probe pulse of classical magnitude. Hence we can safely linearise the system of equations. Splitting each operator \hat{O} into an expectation value \bar{O} (here, $\alpha = \bar{a}$ and $\beta = \bar{b}$) and a zero-mean quantum fluctuation $\delta\hat{O}$ ($\langle \delta\hat{O} \rangle = 0$) and omitting quadratic terms in the fluctuations, we obtain two sets of differential equations: one set for the quantum fluctuations,

$$\left\{ \begin{array}{l} \partial_t \delta\hat{c}(t) = -i\Omega \delta\hat{c}(t) + i \frac{g}{\sqrt{2}} (\alpha^*(t) \delta\hat{a}(t) + \alpha(t) \delta\hat{a}^\dagger(t)), \\ \partial_t \delta\hat{a}(t) = -i\Delta \delta\hat{a}(t) + i \frac{g}{\sqrt{2}} \alpha(t) (\delta\hat{c}^\dagger(t) + \delta\hat{c}(t)) + i \frac{g}{\sqrt{2}} \delta\hat{a}(t) (\bar{c}^*(t) + \bar{c}(t)) - \sqrt{\frac{\kappa}{2\pi}} \int d\omega \delta\hat{b}(\omega, t), \\ \partial_t \delta\hat{b}(\omega, t) = -i(\omega - \omega_L) \delta\hat{b}(\omega, t) + \sqrt{\frac{\kappa}{2\pi}} \delta\hat{a}(t); \end{array} \right. \quad (\text{B2})$$

and one for the classical averages,

$$\left\{ \begin{array}{l} \partial_t \bar{c}(t) = -i\Omega \bar{c}(t) + i \frac{g}{\sqrt{2}} |\alpha(t)|^2, \\ \partial_t \alpha(t) = -i\Delta \alpha(t) + i \frac{g}{\sqrt{2}} \alpha(t) (\bar{c}^*(t) + \bar{c}(t)) - \sqrt{\frac{\kappa}{2\pi}} \int d\omega \beta(\omega, t), \\ \partial_t \beta(\omega, t) = -i(\omega - \omega_L) \beta(\omega, t) + \sqrt{\frac{\kappa}{2\pi}} \alpha(t). \end{array} \right. \quad (\text{B3})$$

Both systems of equations of motion can be solved.

1. Solution for classical averages

For the classical average, we take the formal solution of the input light field $\beta(\omega, t) = e^{-i(\omega-\omega_L)(t-t_0)}\beta(\omega, t_0) + \sqrt{\kappa/(2\pi)} \int_{t_0}^t dt' e^{-i(\omega-\omega_L)(t-t')} \alpha(t')$ and we substitute it in the differential equation for the cavity field α to get

$$\partial_t \alpha(t) = \left[-i\Delta + ig\bar{q}(t) - \frac{\kappa}{2} \right] \alpha(t) - \sqrt{\kappa}\beta(t) \quad (\text{B4})$$

where $\bar{q}(t) = (\bar{c}^*(t) + \bar{c}(t))/\sqrt{2}$ is the mechanical position displacement and $\beta(t) = \sqrt{1/(2\pi)} \int d\omega e^{-i(\omega-\omega_L)(t-t_0)} \beta(\omega, t_0)$ corresponds to the input laser pulse centered around $t = 0$, as defined in the main text. The mechanical displacement is obtained by solving the equation for $\bar{c}(t)$, which splits into a term of zeroth order and a term of first order in the optomechanical strength g ,

$$\bar{c}(t) = \bar{c}(t_0)e^{-i\Omega(t-t_0)} + i\frac{g}{\sqrt{2}} \int_{t_0}^t dt' e^{-i\Omega(t-t')} |\alpha(t')|^2. \quad (\text{B5})$$

We split the position displacement into the respective contributions, $\bar{q}(t) = \bar{q}^{(0)}(t) + \bar{q}^{(1)}(t)$, with

$$\begin{aligned} \bar{q}^{(0)}(t) &= \frac{\bar{c}(t_0)e^{-i\Omega(t-t_0)} + \bar{c}^*(t_0)e^{i\Omega(t-t_0)}}{\sqrt{2}}, \\ \bar{q}^{(1)}(t) &= g \int_{t_0}^t dt' \sin(\Omega(t-t')) |\alpha(t')|^2 \approx g \sin(\Omega t) \int_{t_0}^t dt' |\alpha(t')|^2. \end{aligned} \quad (\text{B6})$$

The approximation holds in the stroboscopic regime in which the mechanical dynamics Ω is slow compared to the duration of the cavity response to the input laser pulse which leads to $|\alpha(t')|$ restricting significant contributions of the integrand to the regime $\Omega t' \ll 1$ around $t' = 0$. Explicitly, the formal solution of the cavity amplitude is,

$$\alpha(t) = \alpha(t_0)e^{-\Gamma(t-t_0)} e^{ig \int_{t_0}^t dt' \bar{q}(t')} - \sqrt{\kappa} \int_{t_0}^t dt' e^{-\Gamma(t-t')} e^{ig \int_{t'}^t dt'' \bar{q}(t'')} \beta(t'), \quad (\text{B7})$$

abbreviating $\Gamma = \kappa/2 + i\Delta$ as before. Since the first term vanishes for $t_0 \rightarrow -\infty$, the amplitude is indeed non-vanishing only for the duration of the laser pulse. Moreover, since the pulse is slow in comparison to the cavity decay time, we can approximate $\beta(t') \approx \beta(t)$ in the second term. This also allows us to approximate $\int_{t'}^t dt'' \bar{q}(t'') \approx \bar{q}(0)(t-t')$ since the mechanical motion is slow compared to both the cavity decay and the pulse and the latter is centered around $t = 0$. Noticing that $\bar{q}^{(1)}(0) \approx 0$, we arrive at the final expression for the cavity amplitude,

$$\alpha(t) \approx -\frac{\sqrt{\kappa}\beta(t)}{\Gamma - ig\bar{q}^{(0)}(0)}. \quad (\text{B8})$$

2. Solution for the quantum fluctuations

The linearised equations of motion (B2) for the quantum fluctuations can be solved analogously. We start with the solution for the light field,

$$\delta\hat{b}(\omega, t) = \delta\hat{b}(\omega, t_0)e^{-i(\omega-\omega_L)(t-t_0)} + \sqrt{\frac{\kappa}{2\pi}} \int_{t_0}^t dt' e^{-i(\omega-\omega_L)(t-t')} \delta\hat{a}(t), \quad (\text{B9})$$

which we substitute into the equation for the cavity field fluctuations,

$$\partial_t \delta\hat{a}(t) = -[\Gamma - ig\bar{q}(t)] \delta\hat{a}(t) + ig\alpha(t) \delta\hat{q}(t) - \sqrt{\kappa} \delta\hat{b}^{(\text{in})}(t), \quad (\text{B10})$$

with $\delta\hat{q}(t) = [\delta\hat{c}(t) + \delta\hat{c}^\dagger(t)]/\sqrt{2}$. Here, the input field operator describes vacuum noise on top of the coherent laser pulse, $\delta\hat{b}^{(\text{in})}(t) = \sqrt{1/2\pi} \int d\omega e^{-i(\omega-\omega_L)(t-t_0)} \delta\hat{b}(\omega, t_0)$. The formal solution is

$$\begin{aligned} \delta\hat{a}(t) &= \delta\hat{a}(t_0)e^{-\int_{t_0}^t dt' (\Gamma - ig\bar{q}(t'))} + \int_{t_0}^t dt' e^{-\Gamma(t-t')+ig \int_{t'}^t dt'' \bar{q}(t'')} \left[ig\alpha(t') \delta\hat{q}(t') - \sqrt{\kappa} \delta\hat{b}^{(\text{in})}(t') \right] \\ &\approx -\sqrt{\kappa} \int_{t_0}^t dt' e^{-[\Gamma - ig\bar{q}(t)](t-t')} \delta\hat{b}^{(\text{in})}(t') + ig\alpha(t) \int_{t_0}^t dt' e^{-[\Gamma - ig\bar{q}^{(0)}(0)](t-t')} \delta\hat{q}(t'), \end{aligned} \quad (\text{B11})$$

which consists of a zeroth order and a first order contribution with respect to g , denoted by $\delta\hat{a}^{(0)}(t)$ and $\delta\hat{a}^{(1)}(t)$, respectively. Here we exploited the fact that the first term in the first line vanishes for $t_0 \rightarrow -\infty$ due to the exponential decay with rate $\kappa/2$, and we made use of the approximations in the stroboscopic regime as before. In particular, $\alpha(t)$ is a Gaussian pulse centered around $t = 0$ that is short compared to the mechanical oscillation time, but long compared to the cavity decay time. To proceed, we need the solution for the mechanical fluctuations,

$$\delta\hat{c}(t) = \delta\hat{c}(t_0)e^{-i\Omega(t-t_0)} + i\frac{g}{\sqrt{2}} \int_{t_0}^t dt' e^{-i\Omega(t-t')} [\alpha(t')\delta\hat{a}^\dagger(t') + \alpha^*(t')\delta\hat{a}(t')], \quad (\text{B12})$$

which again splits into a zeroth order and a first order contribution. In terms of the position fluctuations, $\delta\hat{q}(t) = \delta\hat{q}^{(0)}(t) + \delta\hat{q}^{(1)}(t)$, these contributions are,

$$\begin{aligned} \delta\hat{q}^{(0)}(t) &= \frac{\delta\hat{c}(t_0)e^{-i\Omega(t-t_0)} + \delta\hat{c}^\dagger(t_0)e^{i\Omega(t-t_0)}}{\sqrt{2}}, \\ \delta\hat{q}^{(1)}(t) &= g \int_{t_0}^t dt' \sin[\Omega(t-t')] [\alpha^*(t')\delta\hat{a}(t') + \alpha(t')\delta\hat{a}^\dagger(t')] \\ &\approx g \sin(\Omega t) \int_{t_0}^t dt' [\alpha^*(t')\delta\hat{a}^{(0)}(t') + \alpha(t')\delta\hat{a}^{(0)\dagger}(t')]. \end{aligned} \quad (\text{B13})$$

In the last line we used the stroboscopic approximation again, and we neglected second-order terms in g by replacing the cavity fluctuation with its zeroth order contribution $\delta\hat{a}^{(0)}$. Upon insertion into Eq. (B11), this amounts to neglecting terms of third order in g . Moreover, we notice that the $\delta\hat{q}^{(1)}$ -contribution to $\delta\hat{a}(t)$ vanishes effectively in the stroboscopic regime, since we can approximate $\sin(\Omega t') \approx \sin(\Omega t)$ under the integral and then $\alpha(t)\sin(\Omega t) \sim O(\Omega\tau)$ is set to zero. This contribution, which represents backaction noise, is thus negligible within the linearised stroboscopic regime. Introducing the abbreviation $G(t) = \Gamma - ig\bar{q}^{(0)}(t)$, we are left with

$$\delta\hat{a}^{(0)}(t) = -\sqrt{\kappa} \int_{t_0}^t dt' e^{-G(t)(t-t')} \delta\hat{b}^{(\text{in})}(t'), \quad \delta\hat{a}^{(1)}(t) = ig\alpha(t) \int_{t_0}^t dt' e^{-G(0)(t-t')} \delta\hat{q}^{(0)}(t'). \quad (\text{B14})$$

3. Displacement vector and covariance matrix

Assuming Gaussian statistics, the output field is fully determined by spectrally or time-resolved average displacements and by the respective covariances between the quantum fluctuations around those displacements. Expressed in terms of the time-domain quadrature vector, $\hat{\mathbf{d}}(t) = (\hat{b}^{(\text{out})}(t), \hat{b}^{(\text{out})\dagger}(t))^\top$, the time-resolved average displacements are simply given by the output amplitudes $\beta^{(\text{out})}(t)$. By virtue of the input-output relation, the latter comprise the input laser pulse and the cavity response, which is approximately given in (B8), so that

$$\mathbf{d}(t) = \langle \hat{\mathbf{d}}(t) \rangle = (\beta(t) + \sqrt{\kappa}\alpha(t), \beta^*(t) + \sqrt{\kappa}\alpha^*(t))^\top \approx -\left(\frac{G^*(0)}{G(0)}\beta(t), \frac{G(0)}{G^*(0)}\beta^*(t)\right)^\top. \quad (\text{B15})$$

The time-resolved covariances are given by the matrix elements,

$$\sigma_{ab}(t_i, t_j) = \langle \{\hat{d}_a(t_i), \hat{d}_b^\dagger(t_j)\} \rangle - 2\langle \hat{d}_a(t_i) \rangle \langle \hat{d}_b^\dagger(t_j) \rangle = \left\langle \left\{ \hat{d}_a(t_i) - d_a(t_i), \hat{d}_b^\dagger(t_j) - d_b^*(t_j) \right\} \right\rangle. \quad (\text{B16})$$

Hence, they depend only on the quantum fluctuations of the output field modes. Explicitly,

$$\begin{aligned} \sigma_{11}(t_i, t_j) &= \sigma_{22}(t_j, t_i) = \langle \delta\hat{b}^{(\text{out})}(t_i)\delta\hat{b}^{(\text{out})\dagger}(t_j) \rangle + \langle \delta\hat{b}^{(\text{out})\dagger}(t_j)\delta\hat{b}^{(\text{out})}(t_i) \rangle, \\ \sigma_{12}(t_i, t_j) &= \sigma_{12}(t_j, t_i) = \sigma_{21}^*(t_i, t_j) = \langle \{\delta\hat{b}^{(\text{out})}(t_i), \delta\hat{b}^{(\text{out})}(t_j)\} \rangle. \end{aligned} \quad (\text{B17})$$

By virtue of the input-output relation, we have

$$\delta\hat{b}^{(\text{out})}(t) = \delta\hat{b}^{(\text{in})}(t) + \sqrt{\kappa}\delta\hat{a}^{(0)}(t) + \sqrt{\kappa}\delta\hat{a}^{(1)}(t). \quad (\text{B18})$$

Inserting the cavity terms from Eq. (B14) allows us to expand the covariances in terms of first and second moments of the input field fluctuations and the unperturbed mechanical fluctuations. Most of these terms vanish, since

$\langle \delta\hat{b}^{(\text{in})\dagger}(t_i)\delta\hat{b}^{(\text{in})}(t_j) \rangle = \langle \delta\hat{b}^{(\text{in})\dagger}(t_i)\delta\hat{b}^{(\text{in})\dagger}(t_j) \rangle = \langle \delta\hat{b}^{(\text{in})}(t_i)\delta\hat{b}^{(\text{in})}(t_j) \rangle = 0$ and $\langle \delta\hat{q}^{(0)}(t) \rangle = 0$. The only non-vanishing moments are either of zeroth order or of second order in g . The zeroth order terms are:

$$\langle \delta\hat{b}^{(\text{in})}(t_j)\delta\hat{b}^{(\text{in})\dagger}(t_i) \rangle = \delta(t_i - t_j), \quad (\text{B19})$$

$$\sqrt{\kappa}\langle \delta\hat{b}^{(\text{in})}(t_j)\delta\hat{a}^{(0)\dagger}(t_i) \rangle = \sqrt{\kappa}\langle \delta\hat{a}^{(0)}(t_i)\delta\hat{b}^{(\text{in})\dagger}(t_j) \rangle^* = -\kappa e^{-G^*(t_i)(t_i - t_j)}\Theta(t_i - t_j), \quad (\text{B20})$$

$$\begin{aligned} \kappa\langle \delta\hat{a}^{(0)}(t_j)\delta\hat{a}^{(0)\dagger}(t_i) \rangle &= \kappa^2\Theta(t_j - t_i)\frac{e^{-G(t_j)(t_j - t_i)}}{G(t_j) + G^*(t_i)} + \kappa^2\Theta(t_i - t_j)\frac{e^{-G^*(t_i)(t_i - t_j)}}{G(t_j) + G^*(t_i)} \\ &\approx \kappa e^{-\kappa|t_j - t_i|/2 - i(\Delta - g\bar{q}^{(0)}(t_i))(t_j - t_i)} \end{aligned} \quad (\text{B21})$$

In the last line, we have exploited the stroboscopic regime once more: the fast exponential decay restricts the difference $|t_i - t_j|$ to small values of order $1/\kappa$ so that we can approximate $G(t_i) \approx G(t_j)$ and thus $G(t_j) + G^*(t_i) \approx \kappa$. Hence, in this regime, we find the following identity that will be important later:

$$\sqrt{\kappa}\langle \delta\hat{b}^{(\text{in})}(t_j)\delta\hat{a}^{(0)\dagger}(t_i) \rangle + \sqrt{\kappa}\langle \delta\hat{a}^{(0)}(t_j)\delta\hat{b}^{(\text{in})\dagger}(t_i) \rangle \approx -\kappa\langle \delta\hat{a}^{(0)}(t_j)\delta\hat{a}^{(0)\dagger}(t_i) \rangle. \quad (\text{B22})$$

The second order terms are mixed second moments of $\delta\hat{a}^{(1)}$ and its adjoint operator at two different times,

$$\kappa\langle \delta\hat{a}^{(1)\dagger}(t_i)\delta\hat{a}^{(1)}(t_j) \rangle = \kappa g^2\alpha^*(t_i)\alpha(t_j)\int_{t_0}^{t_i} dt_1 e^{-G(0)(t_i - t_1)}\int_{t_0}^{t_j} dt_2 e^{-G^*(0)(t_j - t_2)}\langle \delta\hat{q}^{(0)}(t_1)\delta\hat{q}^{(0)}(t_2) \rangle, \quad (\text{B23})$$

$$\kappa\langle \delta\hat{a}^{(1)}(t_j)\delta\hat{a}^{(1)\dagger}(t_i) \rangle = \kappa g^2\alpha(t_j)\alpha^*(t_i)\int_{t_0}^{t_j} dt_1 e^{-G(0)(t_j - t_1)}\int_{t_0}^{t_i} dt_2 e^{-G^*(0)(t_i - t_2)}\langle \delta\hat{q}^{(0)}(t_1)\delta\hat{q}^{(0)}(t_2) \rangle, \quad (\text{B24})$$

$$\kappa\langle \delta\hat{a}^{(1)}(t_i)\delta\hat{a}^{(1)}(t_j) \rangle = -\kappa g^2\alpha(t_i)\alpha(t_j)\int_{t_0}^{t_i} dt_1 e^{-G(0)(t_i - t_1)}\int_{t_0}^{t_j} dt_2 e^{-G(0)(t_j - t_2)}\langle \delta\hat{q}^{(0)}(t_1)\delta\hat{q}^{(0)}(t_2) \rangle. \quad (\text{B25})$$

They all depend on two-time correlations of the mechanical position fluctuations, $\langle \delta\hat{q}^{(0)}(t_1)\delta\hat{q}^{(0)}(t_2) \rangle$, with respect to the displaced thermal state we assume for the mechanical mode. These are given by the respective correlations of the full position operators with respect to the undisplaced thermal (Gibbs) state,

$$\langle \delta\hat{q}^{(0)}(t_1)\delta\hat{q}^{(0)}(t_2) \rangle = \text{Tr}[\rho_{\text{th}}\hat{q}^{(0)}(t_1)\hat{q}^{(0)}(t_2)] = \bar{n}\cos\Omega(t_1 - t_2) + \frac{1}{2}e^{-i\Omega(t_1 - t_2)}, \quad (\text{B26})$$

with $\bar{n} = [\exp(\hbar\Omega/k_B T) - 1]^{-1}$ the thermal occupation number. As the correlations oscillate with the slow mechanical frequency, we can invoke the stroboscopic regime again and approximate their time arguments by $(t_1, t_2) \approx (0, 0)$ due to the fast cavity decay and the short pulse duration in Eqs. (B23)-(B25). Hence,

$$\kappa\langle \delta\hat{a}^{(1)\dagger}(t_i)\delta\hat{a}^{(1)}(t_j) \rangle \approx \frac{\kappa g^2}{|G(0)|^2}\alpha^*(t_i)\alpha(t_j)\frac{2\bar{n} + 1}{2} \approx \kappa\langle \delta\hat{a}^{(1)}(t_j)\delta\hat{a}^{(1)\dagger}(t_i) \rangle, \quad (\text{B27})$$

$$\kappa\langle \delta\hat{a}^{(1)}(t_i)\delta\hat{a}^{(1)}(t_j) \rangle \approx -\frac{\kappa g^2}{|G(0)|^2}\alpha(t_i)\alpha(t_j)\frac{2\bar{n} + 1}{2}. \quad (\text{B28})$$

We can now gather all the non-vanishing moments to obtain expressions for the covariance matrix elements in (B17). For σ_{11} , we get

$$\begin{aligned} \sigma_{11}(t_i, t_j) &= \langle \delta\hat{b}^{(\text{in})}(t_i)\delta\hat{b}^{(\text{in})\dagger}(t_j) \rangle + \kappa\left[\langle \delta\hat{a}^{(1)\dagger}(t_j)\delta\hat{a}^{(1)}(t_i) \rangle + \langle \delta\hat{a}^{(1)}(t_i)\delta\hat{a}^{(1)\dagger}(t_j) \rangle\right] \\ &\quad + \sqrt{\kappa}\langle \delta\hat{a}^{(0)}(t_i)\delta\hat{b}^{(\text{in})\dagger}(t_j) \rangle + \sqrt{\kappa}\langle \delta\hat{b}^{(\text{in})}(t_i)\delta\hat{a}^{(0)\dagger}(t_j) \rangle + \kappa\langle \delta\hat{a}^{(0)}(t_i)\delta\hat{a}^{(0)\dagger}(t_j) \rangle \\ &\approx \delta(t_i - t_j) + (2\bar{n} + 1)\frac{\kappa g^2}{|G(0)|^2}\alpha^*(t_j)\alpha(t_i) \approx \delta(t_i - t_j) + (2\bar{n} + 1)\frac{\kappa^2 g^2}{|\Gamma|^4}\beta^*(t_j)\beta(t_i). \end{aligned} \quad (\text{B29})$$

Here, we made use of Eq. (B22) to cancel the second line, we inserted the approximate expression (B8) for the cavity amplitude, and we consistently omitted terms higher than second order in g by replacing $G(0)$ with Γ . Similarly, for σ_{12} we obtain

$$\sigma_{12}(t_i, t_j) = \kappa\langle \{\delta\hat{a}^{(1)}(t_i), \delta\hat{a}^{(1)}(t_j)\} \rangle \approx -(2\bar{n} + 1)\frac{\kappa g^2}{|G(0)|^2}\alpha(t_j)\alpha(t_i) \approx -(2\bar{n} + 1)\frac{\kappa^2 g^2}{\Gamma^4}\beta(t_j)\beta(t_i). \quad (\text{B30})$$

The remaining two matrix elements σ_{22} and σ_{21} are related to the given ones through Eq. (B17). In the limit $g \rightarrow 0$, the covariance matrix reduces to the trivial one for the free mode continuum, as expected.

4. Quantum Fisher Information

To evaluate the QFI with respect to the signal strength parameter ϑ , as defined in Eq. (24), the inverse of the covariance matrix is required. Since obtaining the exact inverse is, in general, not tractable, we assume an expansion of the covariance matrix and subsequently verify that the resulting corrections to the QFI induced by thermal noise remain small. Moreover, when this noise contribution is indeed negligible, its effect for N oscillators can be treated as additive, such that the overall enhancement is only marginally affected. We expand the covariance matrix as $\sigma \approx \sigma_0 + \delta\sigma$, with σ_0 the free (noise- and coupling-free) covariance matrix, assumed non-singular. Writing $\sigma \approx \sigma_0(\mathbb{I} + \sigma_0^{-1}\delta\sigma)$, its inverse follows from the Neumann series: $\sigma^{-1} \approx (\mathbb{I} + \sigma_0^{-1}\delta\sigma)^{-1}\sigma_0^{-1} = \sum_{k=0}^{\infty} (-\sigma_0^{-1}\delta\sigma)^k \sigma_0^{-1} = (\mathbb{I} - \sigma_0^{-1}\delta\sigma + \dots)\sigma_0^{-1}$, which can be truncated to get the approximation $\sigma^{-1} \approx \sigma_0^{-1} - \sigma_0^{-1}\delta\sigma\sigma_0^{-1}$. For the free field, $\sigma_0 = \mathbb{I}$, so that we can approximate the QFI as

$$\mathcal{H} = 2 \int dt |\partial_{\vartheta} \mathbf{d}(t)|^2 - 2 \iint dt_1 dt_2 [\partial_{\vartheta} \mathbf{d}(t_1)]^\dagger \delta\sigma(t_1, t_2) \partial_{\vartheta} \mathbf{d}(t_2) =: \mathcal{H}_0 + \delta\mathcal{H}, \quad (\text{B31})$$

where the first term \mathcal{H}_0 corresponds to the QFI in the absence of thermal and back-action noise and the second term $\delta\mathcal{H}$ represents the correction due to thermal noise, which we obtained in the previous subsection (showing also that back action noise is negligible). Notice that there would be an additional contribution to the QFI coming from the ϑ -dependence of $\delta\sigma$. However, we showed that this dependence is of higher than second order in the optomechanical coupling g and can therefore omit it.

The signal strength parameter ϑ thus enters the QFI only through the derivative of the displacement vector (B15). Assuming, as in the main text, that ϑ describes the signal amplitude up to a proportionality constant, we set $\bar{q}(0) = Q\vartheta$ and arrive at

$$\partial_{\vartheta} \mathbf{d}(t) \approx \left(-\frac{ig\kappa Q}{\Gamma^2} \beta(t), \frac{ig\kappa Q}{\Gamma^{*2}} \beta^*(t) \right)^\top, \quad (\text{B32})$$

dropping higher order contributions of g again, consistently. For a Gaussian input pulse, $\beta(t) = \bar{\beta}e^{-t^2/2\tau^2}$, the free-field QFI without thermal noise simplifies to

$$\mathcal{H}_0 = \frac{4g^2\kappa^2Q^2}{|\Gamma|^4} N_{\text{in}} = \frac{64g^2\kappa^2Q^2}{(\kappa^2 + 4\Delta^2)^2} N_{\text{in}}, \quad (\text{B33})$$

with $N_{\text{in}} = \bar{\beta}^2\tau\sqrt{\pi}$ the total number of photons in the input pulse. For the noise correction of the QFI, we can make use of $d_2(t) = d_1^*(t)$ and the symmetry properties of the covariance matrix in (B17), which leaves us with

$$\begin{aligned} \delta\mathcal{H} &= -4 \iint dt_1 dt_2 \delta\sigma_{11}(t_1, t_2) \partial_{\vartheta} d_1^*(t_1) \partial_{\vartheta} d_1(t_2) - 4\text{Re} \iint dt_1 dt_2 \delta\sigma_{12}(t_1, t_2) \partial_{\vartheta} d_1^*(t_1) \partial_{\vartheta} d_2(t_2) \\ &= -(2\bar{n} + 1) \frac{8g^4\kappa^4Q^2}{|\Gamma|^8} N_{\text{in}}^2 = -\frac{2\bar{n} + 1}{2Q^2} \mathcal{H}_0^2. \end{aligned} \quad (\text{B34})$$

The correction is always negative, as the thermal noise deteriorates coherence and thus reduces phase sensitivity.

We can distinguish two limiting cases. In the low-temperature regime, $k_B T \ll \hbar\Omega$, we have $\bar{n} \approx 0$, and the mechanical zero-point fluctuations diminish the QFI by the small constant fraction $|\delta\mathcal{H}/\mathcal{H}_0| \approx \mathcal{H}_0/2Q^2$. In the relevant weak-signal limit, this relative correction would also be small. More realistically, for low oscillator frequencies and comparably high temperatures, $k_B T \gg \hbar\Omega$, we have $2\bar{n} + 1 \approx 2k_B T/\hbar\Omega$, and the relative correction is $|\delta\mathcal{H}/\mathcal{H}_0| \approx \mathcal{H}_0 k_B T/\hbar\Omega Q^2$.

This gives a condition under which we can safely neglect the contributions of thermal fluctuations of the mechanical element to the covariance matrix of the output light field. It is

$$T \ll T_{\text{max}} = \frac{Q^2\hbar\Omega}{k_B \mathcal{H}_0}. \quad (\text{B35})$$

We consider typical optomechanical parameters, namely $\kappa/2\pi \approx 10^6$ Hz, $\Omega/2\pi \approx 10^3$ Hz, $\Delta \approx \Omega$. Working in the weak-coupling regime with $g/2\pi \approx 1$ Hz and taking $N_{\text{in}} \approx 100$, we further set the mechanical signal parameters to $Q = 1$ and $\varphi = 0$ without loss of generality. For this choice of parameters, we obtain $T_{\text{max}} \approx 7.5$ K. In this case, $T \ll T_{\text{max}}$ can be achieved with simple cooling techniques.

Optomechanical test of the schrödinger-newton equation, Phys. Rev. D **93**, 096003 (2016).

[3] M. Bahrami, M. Paternostro, A. Bassi, and H. Ulbricht, Proposal for a noninterferometric test of collapse models in optomechanical systems, Phys. Rev. Lett. **112**, 210404 (2014).

[4] D. Carney, A. Hook, Z. Liu, J. M. Taylor, and Y. Zhao, Ultralight dark matter detection with mechanical quantum sensors, New J. Phys. **23**, 023041 (2021).

[5] S. Nimmrichter, K. Hornberger, and K. Hammerer, Optomechanical sensing of spontaneous wave-function collapse, Phys. Rev. Lett. **113**, 020405 (2014).

[6] S. Bose, I. Fuentes, A. A. Geraci, S. M. Khan, S. Qvarfort, M. Rademacher, M. Rashid, M. Toroš, H. Ulbricht, and C. C. Wanjura, Massive quantum systems as interfaces of quantum mechanics and gravity, Rev. Mod. Phys. **97**, 015003 (2025).

[7] D. Braun, M. M. Marchese, S. Nimmrichter, S. Qvarfort, D. Rätzel, and H. Ulbricht, Metrology of gravitational effects with mechanical quantum systems (2025), arXiv:2501.18274 [quant-ph].

[8] S. Qvarfort, A. Serafini, P. F. Barker, and S. Bose, Gravimetry through non-linear optomechanics, Nat. Commun. **9**, 3690 (2018).

[9] F. Schneiter, S. Qvarfort, A. Serafini, A. Xuereb, D. Braun, D. Rätzel, and D. E. Bruschi, Optimal estimation with quantum optomechanical systems in the nonlinear regime, Phys. Rev. A **101**, 033834 (2020).

[10] S. Qvarfort, A. D. K. Plato, D. E. Bruschi, F. Schneiter, D. Braun, A. Serafini, and D. Rätzel, Optimal estimation of time-dependent gravitational fields with quantum optomechanical systems, Phys. Rev. Res. **3**, 013159 (2021).

[11] T. J. Kippenberg and K. J. Vahala, Cavity optomechanics: Back-action at the mesoscale, Science **321**, 1172 (2008).

[12] K. Iwasawa, K. Makino, H. Yonezawa, M. Tsang, A. Davidovic, E. Huntington, and A. Furusawa, Quantum-limited mirror-motion estimation, Phys. Rev. Lett. **111**, 163602 (2013).

[13] M. Tsang, Quantum metrology with open dynamical systems, New J. Phys. **15**, 073005 (2013).

[14] S. Bose, A. Mazumdar, G. W. Morley, H. Ulbricht, M. Toroš, M. Paternostro, A. A. Geraci, P. F. Barker, M. S. Kim, and G. Milburn, Spin entanglement witness for quantum gravity, Phys. Rev. Lett. **119**, 240401 (2017).

[15] C. Marletto and V. Vedral, Gravitationally induced entanglement between two massive particles is sufficient evidence of quantum effects in gravity, Phys. Rev. Lett. **119**, 240402 (2017).

[16] T. Krishnanda, G. Y. Tham, M. Paternostro, and T. Paterek, Observable quantum entanglement due to gravity, npj Quantum Inf. **6**, 12 (2020).

[17] M. Carlesso, A. Bassi, M. Paternostro, and H. Ulbricht, Testing the gravitational field generated by a quantum superposition, New J. Phys. **21**, 093052 (2019).

[18] D. Miki, A. Matsumura, and K. Yamamoto, Quantum signature of gravity in optomechanical systems with conditional measurement, Phys. Rev. D **109**, 064090 (2024).

[19] J. Qin, D. W. P. Amaral, S. A. Bhave, E. Cai, D. Carney, R. F. Lang, S. Li, A. M. Marino, G. Marocco, C. Marvinney, J. R. Newton, J. M. Taylor, and C. Tunnell, Mechanical sensors for ultraheavy dark matter searches via long-range forces, Phys. Rev. D **112**, 072003 (2025).

[20] D. Carney, G. Krnjaic, D. C. Moore, C. A. Regal, G. Afek, S. Bhav, B. Brubaker, T. Corbitt, J. Cripe, N. Crisost, *et al.*, Mechanical quantum sensing in the search for dark matter, Quantum Science and Technology **6**, 024002 (2021).

[21] F. Monteiro, G. Afek, D. Carney, G. Krnjaic, J. Wang, and D. C. Moore, Search for composite dark matter with optically levitated sensors, Phys. Rev. Lett. **125**, 181102 (2020).

[22] A. Arvanitaki and A. A. Geraci, Detecting high-frequency gravitational waves with optically levitated sensors, Phys. Rev. Lett. **110**, 071105 (2013).

[23] V. Giovannetti, S. Lloyd, and L. Maccone, Quantum-enhanced measurements: Beating the standard quantum limit, Science **306**, 1330 (2004).

[24] D. Leibfried, E. Knill, S. Seidelin, J. Britton, R. B. Blakestad, J. Chiaverini, D. B. Hume, W. M. Itano, J. D. Jost, C. Langer, *et al.*, Creation of a six-atom ‘schrödinger cat’ state, Nature **438**, 639 (2005).

[25] T. Nagata, R. Okamoto, J. L. O’Brien, K. Sasaki, and S. Takeuchi, Beating the standard quantum limit with four-entangled photons, Science **316**, 726 (2007).

[26] J. M. E. Fraïssé and D. Braun, Coherent averaging, Ann. Phys. (Berlin) **527**, 701 (2015).

[27] D. Braun, G. Adesso, F. Benatti, R. Floreanini, U. Marzolino, M. W. Mitchell, and S. Pirandola, Quantum-enhanced measurements without entanglement, Rev. Mod. Phys. **90**, 035006 (2018).

[28] D. Braun and S. Popescu, Coherently enhanced measurements in classical mechanics, Quantum Meas. Quantum Metrol. **2**, 000010247820140003 (2014).

[29] S. Boixo, S. T. Flammia, C. M. Caves, and J. Geremia, Generalized limits for single-parameter quantum estimation, Phys. Rev. Lett. **98**, 090401 (2007).

[30] J. Beltrán and A. Luis, Breaking the heisenberg limit with inefficient detectors, Phys. Rev. A **72**, 045801 (2005).

[31] B. L. Higgins, D. W. Berry, S. D. Bartlett, H. M. Wiseman, and G. J. Pryde, Entanglement-free heisenberg-limited phase estimation, Nature **450**, 393 (2007).

[32] U. Marzolino and D. Braun, Precision measurements of temperature and chemical potential of quantum gases, Phys. Rev. A **88**, 063609 (2013).

[33] T. Juffmann, B. B. Klopfer, T. L. Frankort, P. Haslinger, and M. A. Kasevich, Multi-pass microscopy, Nat. Commun. **7**, 12858 (2016).

[34] S. Nimmrichter, C.-F. Chen, B. B. Klopfer, M. A. Kasevich, and T. Juffmann, Full-field cavity enhanced microscopy techniques, J. Phys. Photonics **1**, 015007 (2018).

[35] C. Gardiner and P. Zoller, *The Quantum World of Ultra-Cold Atoms and Light Book III: Ultra-Cold Atoms* (World Scientific, 2017).

[36] S. M. Dutra, *Cavity quantum electrodynamics: the strange theory of light in a box* (John Wiley & Sons, Ltd, 2005).

[37] C. W. Gardiner and M. J. Collett, Input and output in damped quantum systems: Quantum stochastic differential equations and the master equation, Phys. Rev. A **31**, 3761 (1985).

[38] M. R. Vanner, I. Pikovski, G. D. Cole, M. S. Kim,

Č. Brukner, K. Hammerer, G. J. Milburn, and M. Aspelmeyer, Pulsed quantum optomechanics, *Proc. Natl. Acad. Sci.* **108**, 16182 (2011).

[39] I. Pikovski, *Macroscopic quantum systems and gravitational phenomena*, Ph.D. thesis, Wien U., Vienna U. (2014).

[40] O. Pinel, P. Jian, N. Treps, C. Fabre, and D. Braun, Quantum parameter estimation using general single-mode gaussian states, *Phys. Rev. A* **88**, 040102 (2013).

[41] D. Šafránek, Estimation of gaussian quantum states, *J. Phys. A: Math. Theor.* **52**, 035304 (2018).

[42] D. Rätzel and R. Schützhold, Decay of quantum sensitivity due to three-body loss in bose-einstein condensates, *Phys. Rev. A* **103**, 063321 (2021).

[43] J. Manley, D. J. Wilson, R. Stump, D. Grin, and S. Singh, Searching for scalar dark matter with compact mechanical resonators, *Phys. Rev. Lett.* **124**, 151301 (2020).

[44] L. Hamaide, H. Banks, P. Barker, and A. A. Geraci, Searching for ultralight dark matter with molequite: a massive optically levitated quantum tabletop experiment (2025), arXiv:2512.00166 [hep-ph].

[45] B. P. Abbott, R. Abbott, T. D. Abbott, M. R. Abernathy, F. Acernese, K. Ackley, C. Adams, T. Adams, P. Adesso, R. X. Adhikari, *et al.* (LIGO Scientific Collaboration and Virgo Collaboration), Observation of gravitational waves from a binary black hole merger, *Phys. Rev. Lett.* **116**, 061102 (2016).

[46] J. S. B. Wyithe and A. Loeb, Low-frequency gravitational waves from massive black hole binaries: predictions for lisa and pulsar timing arrays, *Astrophys. J.* **590**, 691 (2003).

[47] P. D. Lasky, Gravitational waves from neutron stars: A review, *Publications of the Astronomical Society of Australia* **32**, e034 (2015).

[48] B. P. Abbott *et al.* (LIGO Scientific Collaboration and Virgo Collaboration), All-sky search for continuous gravitational waves from isolated neutron stars using advanced ligo o2 data, *Phys. Rev. D* **100**, 024004 (2019).

[49] V. Dergachev and M. A. Papa, Results from high-frequency all-sky search for continuous gravitational waves from small-ellipticity sources, *Phys. Rev. D* **103**, 063019 (2021).

[50] N. Christensen, Stochastic gravitational wave backgrounds, *Rep. Prog. Phys.* **82**, 016903 (2018).

[51] M. Goryachev and M. E. Tobar, Gravitational wave detection with high frequency phonon trapping acoustic cavities, *Phys. Rev. D* **90**, 102005 (2014).

[52] S. Singh, L. A. D. Lorenzo, I. Pikovski, and K. C. Schwab, Detecting continuous gravitational waves with superfluid 4he, *New J. Phys.* **19**, 073023 (2017).

[53] M. Goryachev, W. M. Campbell, I. S. Heng, S. Galliou, E. N. Ivanov, and M. E. Tobar, Rare events detected with a bulk acoustic wave high frequency gravitational wave antenna, *Phys. Rev. Lett.* **127**, 071102 (2021).

[54] M. A. Page, M. Goryachev, H. Miao, Y. Chen, Y. Ma, D. Mason, M. Rossi, C. D. Blair, L. Ju, D. G. Blair, *et al.*, Gravitational wave detectors with broadband high frequency sensitivity, *Communications Physics* **4**, 27 (2021).

[55] G. Tobar, I. Pikovski, and M. E. Tobar, Detecting khz gravitons from a neutron star merger with a multi-mode resonant mass detector, *Classical and Quantum Gravity* **42**, 055017 (2025).

[56] M. Maggiore, *Gravitational Waves: Volume 1: Theory and Experiments* (Oxford University Press, 2007).

[57] D. Rätzel and I. Fuentes, Testing small scale gravitational wave detectors with dynamical mass distributions, *J. Phys. Commun.* **3**, 025009 (2019).

[58] A. Shoda, M. Ando, K. Ishidoshiro, K. Okada, W. Kokuyama, Y. Aso, and K. Tsubono, Search for a stochastic gravitational-wave background using a pair of torsion-bar antennas, *Phys. Rev. D* **89**, 027101 (2014).

[59] A. Patra, L. Aiello, A. Ejlli, W. L. Griffiths, A. L. James, N. Kuntimaddi, O. Kwon, E. Schwartz, H. Vahlbruch, S. M. Vermeulen, K. Kokeyama, K. L. Dooley, and H. Grote, Broadband limits on stochastic length fluctuations from a pair of table-top interferometers, *Phys. Rev. Lett.* **135**, 101402 (2025).

[60] F. Spengler, D. Rätzel, and D. Braun, Perspectives of measuring gravitational effects of laser light and particle beams, *New J. Phys.* **24**, 053021 (2022).

[61] D. Braun, R. Cai, P. Hermes, M. M. Marchese, S. Nimmrichter, C. Pfeifer, D. Rätzel, S. Redaelli, and H. Ulbricht, The path towards measuring the gravitational field of proton bunches at accelerators (2025), arXiv:2504.10942 [hep-ex].

[62] C. Pfeifer, D. Rätzel, and D. Braun, Gravitational attraction of ultrarelativistic matter: A new testbed for modified gravity at the large hadron collider, *Phys. Rev. D* **111**, 084073 (2025).